



HAL
open science

Structural insights into perilipin 3 membrane association in response to diacylglycerol accumulation

Yong Mi Choi, Dalila Ajjaji, Kaelin Fleming, Peter Borbat, Meredith Jenkins,
Brandon Moeller, Shaveen Fernando, Surita Bhatia, Jack Freed, John Burke,
et al.

► To cite this version:

Yong Mi Choi, Dalila Ajjaji, Kaelin Fleming, Peter Borbat, Meredith Jenkins, et al.. Structural insights into perilipin 3 membrane association in response to diacylglycerol accumulation. *Nature Communications*, 2023, 14 (1), pp.3204. 10.1038/s41467-023-38725-w . hal-04234703

HAL Id: hal-04234703

<https://hal.science/hal-04234703>

Submitted on 10 Oct 2023

HAL is a multi-disciplinary open access archive for the deposit and dissemination of scientific research documents, whether they are published or not. The documents may come from teaching and research institutions in France or abroad, or from public or private research centers.

L'archive ouverte pluridisciplinaire **HAL**, est destinée au dépôt et à la diffusion de documents scientifiques de niveau recherche, publiés ou non, émanant des établissements d'enseignement et de recherche français ou étrangers, des laboratoires publics ou privés.



Distributed under a Creative Commons Attribution 4.0 International License

1
2
3
4 **Structure and dynamics of human perilipin 3 membrane association**
5

6 Yong Mi Choi^{1a}, Dalila Ajjaji^{2a}, Kaelin D. Fleming³, Peter P. Borbat^{4,5}, Meredith L. Jenkins³,
7 Brandon E Moeller³, Shaveen Fernando⁶, Surita Bhatia⁶, Jack H. Freed^{4,5}, John E. Burke^{3,7*},
8 Abdou Rachid Thiam^{2*}, Michael V. Airola^{1*}
9

10
11 ¹Department of Biochemistry and Cell Biology, Stony Brook University, Stony Brook NY 11794, USA

12 ²Laboratoire de Physique de l'École normale supérieure, ENS, Université PSL, CNRS, Sorbonne
13 Université, Université Paris Cité, F-75005 Paris, France

14 ³Department of Biochemistry and Microbiology, University of Victoria, Victoria BC V8N 1A1, Canada

15 ⁴National Biomedical Resource for Advanced Electron Spin Resonance Technology (ACERT), Cornell
16 University, Ithaca NY 14853, USA

17 ⁵Department of Chemistry and Chemical Biology, Cornell University, Ithaca NY 14853, USA

18 ⁶Department of Chemistry, Stony Brook University, Stony Brook NY 11794, USA

19 ⁷Department of Biochemistry and Molecular Biology, The University of British Columbia, Vancouver,
20 British Columbia V6T 1Z3, Canada

21
22
23 ^aThese authors contributed equally
24

25
26 *Address correspondence to:

27 Michael V. Airola, michael.airola@stonybrook.edu

28 Abdou Rachid Thiam, thiam@ens.fr

29 John E. Burke, jeburke@uvic.ca
30

31
32
33
34 **ABSTRACT**

35 Lipid droplets (LDs) are dynamic organelles that contain an oil core mainly composed of
36 triglycerides (TAG) that is surrounded by a phospholipid monolayer and LD-associated proteins
37 called perilipins (PLINs). During LD biogenesis, perilipin 3 (PLIN3) is recruited to nascent LDs
38 as they emerge from the endoplasmic reticulum. Here, we analyzed how lipid composition
39 affects PLIN3 recruitment to membrane bilayers and LDs, and the structural changes that occur
40 upon membrane binding. We found the TAG precursors phosphatidic acid and diacylglycerol
41 (DAG) recruit PLIN3 to membrane bilayers and define an expanded Perilipin-ADRP-Tip47 (PAT)
42 domain that preferentially binds DAG enriched membranes. Membrane binding induces a
43 disorder/order transition of alpha helices within the PAT domain and 11-mer repeats, with
44 intramolecular distance measurements consistent with the expanded PAT domain adopting a
45 folded but dynamic structure upon membrane binding. In cells, PLIN3 is recruited to DAG
46 enriched ER membranes, and this requires both the PAT domain and 11-mer repeats. This
47 provides molecular details of PLIN3 recruitment to nascent LDs and identifies a function of the
48 PAT domain of PLIN3 in DAG binding.

49

50 INTRODUCTION

51 Lipid droplets (LDs) act as energy reservoirs in cells. They contain a neutral lipid core of mainly
52 triacylglycerols (TAGs) and cholesterol esters with a phospholipid monolayer that surrounds the
53 neutral lipid core. This creates a membrane environment for LDs that is distinct from membrane
54 bilayers and recruits several LD-associated proteins [1-3]. In addition to a major role in energy
55 storage, LDs are also important cellular hubs that traffic proteins and lipids between organelles,
56 regulate ER stress, and contribute to viral infections [4-6].

57

58 LDs are formed in the ER where neutral lipids are synthesized [7, 8]. Mechanistically, LD
59 formation involves several steps [9] including accumulation of neutral lipids in the outer ER
60 membrane leaflet, neutral lipid nucleation aided by the seipin complex and associated factors
61 (e.g. LDAF1) [10], formation of nascent LDs that bud from the ER [11, 12] and LD growth and
62 maturation [13, 14]. Several lines of evidence support the idea that the phospholipid
63 composition of the ER membrane is locally edited to promote LD assembly or recruit specific
64 proteins important for LD formation such as seipin and ORP proteins [7, 15-17]. Although there
65 is still uncertainty regarding the phospholipid composition at the initial stages of LD formation,
66 evidence from yeast suggest diacylglycerol (DAG), the direct precursor of TAG, is enriched in
67 discrete ER subdomains where LD biogenesis is initiated [15, 18]. DAG can also promote TAG
68 nucleation and impact the architecture of LDs on the ER [15, 19].

69

70 Perilipins (PLINs) are the major class of proteins that coat the surface of LDs [20-26]. There are
71 five PLINs in humans that bind LDs at various stages of their initiation and maturation [21]. For
72 example, PLIN1 is the major PLIN that binds to mature LDs in adipocytes, while PLIN2 and
73 PLIN5 reside on mature LDs in liver and muscle cells, respectively [27]. In contrast, PLIN3
74 displays near ubiquitous expression and binds to early LDs as they bud from the ER but is later
75 displaced by other PLINs as LDs grow and mature [10, 28]. PLIN3 is stable and not degraded in
76 the absence of LDs. This allows PLIN3 to translocate from the cytoplasm to sites of early LD
77 formation, where PLIN3 is well established to act as a marker for the biogenesis of early LDs
78 across species [10, 28, 29].

79

80 PLINs share a conserved protein domain architecture composed of an N-terminal PAT domain,
81 followed by variable stretches of 11-mer repeats and a C-terminal 4-helix bundle [30, 31]. The
82 11-mer repeats form amphipathic helices that are sufficient to recruit PLINs to LDs [30-32],
83 while the 4-helix bundle in some PLINs can also bind LDs [30, 33]. The binding of amphipathic

84 helices, such as those found in the 11-mer repeats, to membrane interfaces is greatly
85 influenced by the level or presence of phospholipid packing defects [34, 35]. The degree of
86 packing is determined by the type of lipid present (as indicated in the triangle in **Fig. 1A**). When
87 it comes to the oil-water interface of LDs, the recruitment of amphipathic helices is greater when
88 the level of phospholipid packing is lower [35, 36], i.e. when there are more packing defects.
89 Although the PAT domain is the most conserved domain among PLINs, its function is not clear,
90 as it has not been demonstrated to bind to membranes or LDs.

91
92 Here, we examine the mechanism of PLIN3 recruitment to membrane bilayers and LDs using a
93 combination of *in vitro* and cell culture assays, and analyze the structural changes induced by
94 membrane binding using hydrogen-deuterium exchange mass spectrometry (HDX-MS) and
95 pulsed-dipolar electron spin resonance spectroscopy (PD-ESR). We found that human PLIN3 is
96 recruited to membrane bilayers enriched in the TAG precursors phosphatidic acid (PA) and
97 DAG. By delineating the roles of the PAT domain and 11-mer repeats, we define an expanded
98 PAT domain that is sufficient for PLIN3 to bind DAG enriched membranes, while the 11-mer
99 repeats are sufficient to bind LD monolayers. We confirm that DAG enrichment can drive PLIN3
100 recruitment to ER membranes in cells, and this requires both the PAT domain and 11-mer
101 repeats. Structurally, the PAT domain and 11-mer repeats form inducible alpha helices to drive
102 membrane association and the PAT domain forms a tertiary structure upon membrane binding.
103 Taken together, this study provides molecular insight into how PLIN3 is recruited to early LDs
104 and reveals a novel function for the PAT domain of PLIN3 in DAG binding.

105
106
107

108 RESULTS

109 The Triglyceride Precursors DAG and PA Recruit PLIN3 to Membrane Bilayers

110 To systematically define how lipid composition affects PLIN3 recruitment to membrane bilayers,
111 we purified recombinant human PLIN3 from *Escherichia coli* and used liposome co-
112 sedimentation assays to monitor membrane binding. Liposomes were prepared using multiple
113 freeze/thaw cycles and characterized by dynamic light scattering (DLS) (**Fig. S1A**). Liposomes
114 were made from phospholipids with different acyl-chain combinations comprised of either
115 palmitoyl-oleoyl (PO) or di-oleoyl (DO) phospholipids (**Fig. 1A**). PO phospholipids have one
116 unsaturated acyl chain and are representative of the typical lipid composition in ER membranes.
117 DO phospholipids contain two unsaturated acyl chains, have increased membrane packing
118 defects [34, 37-39] and are enriched in ER membranes after oleate supplementation, which
119 stimulates LD formation [15, 40-42]. Initial liposome co-sedimentation experiments varied the
120 ratio of neutral phospholipids phosphatidylcholine (PC) and phosphatidylethanolamine (PE), as
121 PC and PE represent the major lipids on both the cytoplasmic face of the ER and surface of LDs,
122 PE increases both PLIN2 binding to liposomes [43] and PLIN3 insertion into mixed lipid
123 monolayers at phospholipid-oil interfaces [44] and the ratio of PC to PE has previously been
124 shown to regulate protein distribution on LDs [43, 45]. Under all PC-to-PE ratios tested, PLIN3
125 did not bind liposomes comprised solely of PC and PE (**Fig. 1B**).

126
127 We next asked whether addition of other lipids that are synthesized in the ER could recruit
128 PLIN3 to membranes by generating PC/PE liposomes containing 20mol% of either phosphatidic
129 acid (PA), phosphatidylserine (PS), diacylglycerol (DAG), phosphatidylinositol (PI) or C18:1
130 ceramide. Regardless of lipid composition, PLIN3 did not bind to any PO-based liposomes (**Fig.**
131 **1C, 1D**). However, PLIN3 was recruited to DO-based liposomes enriched in DAG or PA [37, 38,
132 46] (**Fig. 1C, 1D**). Addition of DOPS and ceramide resulted in a minor increase in PLIN3 binding
133 in DO-based liposomes, while the addition of PI had no effect (**Fig. 1C, 1D**).

134
135 PLIN3 recruitment to DO-based liposomes depended on the surface concentration of DAG, with
136 5mol% DAG able to induce ~10% binding, and 20mol% DAG inducing 35% binding (**Fig. 1E**).
137 The addition of DOPA further increased PLIN3 binding in DAG-containing liposomes, which
138 suggested a synergistic effect of PA and DAG on PLIN3 membrane recruitment (**Fig. 1F**).
139 Increasing the total liposome concentration caused the majority of PLIN3 to bind membranes,
140 but 5% of PLIN3 remained in the soluble fraction (**Fig. S2A**). DLS characterization indicated
141 DAG enriched liposomes had two populations based on size (**Fig. S1C, S1D**), which is likely

142 due to the fusogenic properties of DAG [46]. The addition of DOPA or PLIN3 protein decreased
143 or eliminated the population of the larger (>400 nm) liposomes (**Fig. S1C, S1D**). We concluded
144 that PLIN3 binds liposomes containing DAG and/or PA, which are notably the membrane-lipid
145 precursors for triglyceride synthesis, and PLIN3 can also remodel membranes, consistent with
146 previous studies [29].

147

148 **PLIN3 Binds to Liposomes with Membrane Packing Defects**

149 LDs have increased membrane packing defects in comparison to membrane bilayers [47].
150 Previously, PLIN4 has been shown to have increased binding to liposomes composed of methyl
151 branched diphytanoyl (4ME) phospholipids that create shallow lipid-packing defects that can be
152 accessed by hydrophobic insertion of peripheral membrane proteins, such as PLINs [31, 48].
153 The packing defects induced by 4ME phospholipids are greater than DO phospholipids because
154 of the wider space between lipids [48]. In comparison to DO and PO liposomes, 4ME
155 phospholipids significantly increased PLIN3 liposome association with ~70% binding observed
156 with a mixture of 4ME-PC and 4ME-PE (**Fig. 1G**). Consistent with our previous observations,
157 4ME-PA further increased PLIN3 binding, while 4ME-PS and C18:1 ceramide decreased
158 binding (**Fig. 1G**). The effect of DAG was unable to be assessed as addition of DAG to 4ME-
159 PC/PE disrupted proper liposome formation. Taken together, this suggests PLIN3 membrane
160 binding is also dependent on lipid packing defects, and PA can further enhance PLIN3
161 membrane binding.

162

163 **PLIN3 Binding to Artificial Lipid Droplets**

164 As the major function of PLIN3 is to bind to emerging LDs as they bud from the ER, we next
165 assessed the ability of recombinant PLIN3 to bind artificial lipid droplets (ALDs) *in vitro* using a
166 flotation assay [10, 28, 29, 49]. ALDs were generated with a triolein neutral lipid core
167 surrounded by a phospholipid monolayer of DOPC and DOPE in 1:2.5 molar ratio of
168 phospholipids to TAG. ALDs with 80mol% DOPC and 20mol% DOPE showed 50% binding of
169 PLIN3 (**Fig. S2B**). The addition of the anionic phospholipids PI4P decreased PLIN3 binding to
170 ALDs. In contrast, PA, PS and PI slightly decreased binding, ceramide did not affect binding,
171 and DAG slightly increased PLIN3 binding. However, none of these effects were statistically
172 significant. The modest impact of these PA, PS, PI, DAG, and ceramide, which all can induce
173 negative curvature or charge in membrane bilayers, may be due to the basal occurrence of
174 significant phospholipid packing voids on the ALD surface as compared with bilayers [36, 47];
175 while the strongly charged PI4P would instead mask these and diminish binding [47].

176

177 **The PAT Domain and 11-mer Repeats are Disordered in the Absence of Membranes**

178 We next sought to examine how the structure of PLIN3 changes upon membrane binding, first
179 focusing on the structure of PLIN3 in the absence of membranes. For these experiments, we
180 used hydrogen deuterium exchange mass spectrometry (HDX-MS), which measures the
181 exchange of amide hydrogens with deuterated solvent. This method acts as a readout for
182 protein conformational dynamics with regions that form secondary structures undergoing slower
183 deuterium exchange than disordered regions, which lack intramolecular hydrogen bonds and
184 secondary structure [50, 51]. A brief pulse of deuterated solvent is useful for identifying regions
185 within a protein that lack structure compared to ordered regions [52, 53].

186

187 We determined the absolute exchange of PLIN3 after a 3sec pulse of deuterium incorporation at
188 0°C (equivalent to ~0.3sec at 20°C) using a fully deuterated control. After the deuterium pulse,
189 the first 200 residues of PLIN3 comprising the PAT domain and 11-mer repeats were fully
190 deuterated, indicating these regions are completely disordered in the absence of membranes
191 **(Fig. 2A)**. The 4-helix bundle and α/β domain were largely ordered with comparatively low rates
192 of deuterium incorporation **(Fig. 2A)**, which is consistent with prior structural studies of PLIN3
193 [54, 55].

194

195 **The PAT Domain and 11-mer Repeats are the Major Drivers of PLIN3 Membrane** 196 **Association**

197 We next sought to determine any conformational changes that occur during membrane binding
198 using HDX-MS. Having established optimal conditions for PLIN3 membrane binding, we
199 measured the deuterium exchange rate over various time points (3, 30, 300, and 3000sec) in
200 the absence or presence of 4ME liposomes composed of 60mol% 4ME-PC, 20mol% 4ME-PE,
201 and 20mol% 4ME-PA.

202

203 In the presence of membranes, striking differences in deuterium exchange were observed
204 throughout the PLIN3 sequence **(Fig. 2E, Table S1, source data)**. The most notable
205 differences were large decreases in deuterium exchange in the PAT domain and 11-mer repeat
206 regions. In comparison to previous results that demonstrated the 11-mer repeats are sufficient
207 for the lipid droplet association [30, 31], this suggests that the PAT domain and 11-mer repeats
208 are both major contributors to membrane binding. Consistently, we found that a purified PAT/11-

209 mer repeats fragment displayed similar membrane recruitment as full length PLIN3 to DO
210 liposomes enriched in DAG and PA, and 4ME liposomes (**Fig. 2C, 2D**).

211

212 The HDX-MS results suggested that membrane binding induces the formation of a secondary
213 structure in the PAT domain and 11-mer repeats. This is consistent with both AlphaFold and
214 RoseTTAFold models that predict the PAT domain and 11-mer repeats form amphipathic alpha
215 helices, with the PAT domain adopting a triangular globular structure and the 11-mer repeats
216 forming a series of extended alpha helices (**Fig. 2B, 3B**). Based on these results we concluded
217 that the PAT domain and 11-mer repeats of PLIN3 are intrinsically disordered in the absence of
218 membranes, with inducible amphipathic alpha helices being stabilized upon membrane binding.

219

220 Notably, many of the peptides with the PAT domain and 11-mer repeats displayed a bimodal
221 distribution of deuterium exchange upon membrane binding (**Fig. S3A, S3B**). This differs from a
222 canonical distribution where the degree of deuteration is gaussian in individual peptides. The
223 observed bimodal distributions are consistent with either EX1 exchange [56], or there being two
224 distinct protein conformations in the sample. Depending on the membrane residency of PLIN3,
225 bimodal distributions can be consistent with observations of the free and membrane bound state.
226 Given our previous observation that the PAT and 11-mer repeats are intrinsically disordered in
227 the absence of membranes, the simplest interpretation is that the PAT domain and 11-mer
228 repeats cycle between two states: 1) a membrane bound alpha helical state on membranes that
229 is strongly protected from H-D exchange and 2) an intrinsically disordered solution state that
230 rapidly exchanges with deuterated solvent upon dissociation from membranes and leads to
231 rapid H-D exchange. Therefore, the half-life of bimodal exchange can act as a surrogate for
232 membrane residency time for disordered regions of the protein.

233

234 The protection from deuterium exchange and the non-gaussian bimodal distribution for most
235 peptides in the PAT domain persisted over a longer time course (~300sec) in comparison to
236 peptides within the 11-mer repeat regions (~30sec) (**Fig. S4A**). This trend of longer HDX
237 protection correlated with the degree of sequence conservation among PLINs (**Fig. 3A**). Taken
238 together this supports a role for the PAT domain in membrane binding and suggests a similar
239 role for the highly conserved PAT domain in other PLINs.

240

241 In contrast to the N-terminal PAT domain and 11-mer repeats, the C-terminal 4-helix bundle
242 displayed a large increase in deuterium exchange (**Fig. 2E, S4A**). The most apparent increase

243 in deuterium exchange was in the middle of the 4-helix bundle. We hypothesized this was due
244 to the 4-helix bundle unfolding upon membrane binding, with this possibly contributing to
245 membrane recruitment. To test this, we examined the ability of a purified PLIN3 4-helix bundle
246 fragment (residues 197-427) to bind membranes. Consistent with our hypotheses, the isolated
247 4-helix bundle bound to the 4ME-PC/PE/PA liposomes that were used in the HDX-MS
248 experiment (**Fig. 2C, 2D**). However, the 4-helix bundle did not bind to 4ME-liposomes lacking
249 PA, or to any DO-based liposomes even when PA and DAG were present (**Fig. 2C, 2D**). We
250 concluded that the 4-helix bundle of PLIN3 can unfold and bind membranes, but only under very
251 specific condition such as the presence of accumulated PA on the membrane having packing
252 defects induced by 4ME-PC/PE. This conclusion is supported by the PA accumulation at the
253 nascent LD formation site where lipid packing defects occur [17].

254
255

256 To understand how lipid composition influences the structure of PLIN3, we again applied HDX-
257 MS, using variable liposome compositions of 4ME-PC/PE and DOPC/PE/DAG (**Fig. 2F, 2G**). In
258 line with of previous HDX-MS and liposome sedimentation experiments, we observed protection
259 from H-D exchange in the PAT domain and 11-mer repeats using 4ME-PC/PE and
260 DOPC/PE/DAG liposomes, with the magnitude and duration of H-D exchange protection in
261 these regions correlating with the observed fraction of PLIN3 bound in liposome sedimentation
262 assays (**Fig. S4B, 1D and 1G**).

263

264 In contrast, with the 4ME-PC/PE and DOPC/PE/DAG lipid compositions, the 4-helix bundle did
265 not display large increases in deuterium exchange indicating that 4-helix bundle is not involved
266 in membrane binding in the absence of PA. Taken together, these results confirm that the PAT
267 domain and 11-mer repeats are the major lipid interacting regions of PLIN3, and that the 4-helix
268 bundle forms a stable tertiary structure that in general does not contribute to membrane
269 association, unless PA is present in membrane areas with shallow lipid packing defects. This
270 condition is particularly fulfilled at nascent LD formation sites.

271

272 **An expanded PAT domain binds DAG enriched membranes**

273 Our results suggested a role for the PAT domain in PLIN3 membrane association. However,
274 several studies [30, 31] have previously established the 11-mer repeats of PLINs are sufficient
275 for membrane binding, and to our knowledge, the PAT domain alone has not been
276 demonstrated to bind membranes. Complicating matters, the precise boundaries of the PAT

277 domain have been difficult to establish. Previous studies have suggested the PAT domain
278 consists of the N-terminal 97 residues in PLIN3 [30], which are highly conserved with other
279 PLINs (**Fig. 3A**). However, high sequence conservation between PLINs continues beyond
280 residue 97 and ends at residue 115 in PLIN3 (**Fig. 3A**). This suggests the PAT domain may be
281 larger than previously expected. Consistent with the sequence conservation, both AlphaFold [57]
282 and RoseTTA fold [58] predict a triangular alpha helical tertiary structure for the PAT domain
283 that encompasses residues 22-116 (**Fig. 3B**).

284

285 To investigate the PAT domain boundaries and membrane interaction capabilities, we purified
286 several C-terminal extended PAT domain constructs and the corresponding 11-mer repeats
287 counterparts (**Fig. 3C**) and assessed the ability of these fragments to bind DO liposomes
288 containing either 20mol% PA or 20mol% DAG. As an important note, we were unable to purify
289 the previously suggested PAT domain construct (residues 1-97), as this construct was not
290 stably expressed in *Escherichia coli*. This is consistent with the poor expression of the PAT
291 domain of PLIN1 in yeast [30].

292

293 In general, fragments encompassing the PAT domain bound strongly to liposomes in the
294 presence of DAG, with modest liposome binding in the presence of PA (**Fig. 3D**). In contrast,
295 the 11-mer repeats bound to liposomes containing either PA or DAG (**Fig. 3D**). Taken together,
296 the data suggests that the PAT region does form a domain that spans residues 22-116 in PLIN3.
297 Notably, this expanded PAT domain is capable of membrane binding and displays a preference
298 for binding DAG enriched membranes, while the 11-mer repeats of PLIN3 do not.

299

300 **Conformational Rearrangements of the PAT Domain upon Membrane Binding**

301 We first sought to confirm the effects of liposome binding on secondary structure of PLIN3 by
302 circular dichroism (CD) (**Fig. S5**). Liposomes were prepared with 4ME-PC/PE/PA, which
303 recruited all the PLIN3 constructs (full length, PAT, 11-mer repeats, PAT/11-mer repeats, 4-helix
304 bundle) in the previous liposome co-sedimentation experiments. For full length PLIN3, the
305 presence of liposomes increased overall helicity as observed by an increased negative peak
306 around 222nm in the CD spectra. In comparison, the CD spectra of the 4-helix bundle was
307 largely unaffected by the presence of liposomes and was consistent with a stable alpha helical
308 structure. In contrast, the PAT/11-mer repeats adopted a mostly random coil structure in
309 solution with a negative peak around 200nm, and a shift to alpha helices in the presence of
310 liposomes as indicated by a large negative peak at 222nm. Liposomes induced similar changes

311 in the CD spectra for both the PAT domain and 11-mer repeats alone. Taken together, this
312 confirms that the increase in helicity observed in full length PLIN3 by membranes was due to
313 the PAT/11-mer repeats undergoing a disorder/alpha helical transition. This is in line with our
314 HDX-MS results and prior studies of PLIN2 and PLIN3 fragments [55, 59].

315
316 Next, to investigate if membranes induced conformational changes in the PAT domain, we
317 applied the pulsed-dipolar spectroscopy (PDS) technique of double electron-electron resonance
318 (DEER) [60, 61] to full length PLIN3 in solution and bound to liposomes. PDS is a collection of
319 several, based on recording electron spin-echo (ESE), pulse ESR techniques [62-66] routinely
320 applied to characterize protein conformations by providing accurate constraints in the distance
321 range of $\sim 10\text{-}90\text{\AA}$. The amplitude of detected ESE depends on dipolar coupling between the
322 spins of unpaired electrons in nitroxide spin labels covalently bound to engineered cysteine
323 residues. Stepping out pulse separation in the sequence produces the time domain ESE
324 envelope, from which the distances could be reconstructed. [62-65].

325
326 Two sets of residues (25 and 96; 37 and 114) were selected for spin labeling, which were
327 respectively 71 and 77 residues apart in the primary sequence but predicted to be in close
328 proximity by AlphaFold and RoseTTAFold (**Fig. 4A-4C**). Comparison of the DEER decoherence
329 (decay) times indicated that the PAT domain is less structured and/or intrinsically disordered in
330 solution versus when bound to liposomes, which is consistent with our HDX-MS and CD
331 analysis (**Fig. 4B, 4D**). One can estimate, based on $\sim 20\%$ extent of decay in solution compared
332 to liposomes that the decoherence time is of the order of $20\mu\text{s}$, which corresponds to nearly a
333 100\AA separation expected for a random polypeptide chain with stiffness [67]. In contrast, with
334 liposomes the decoherence times are fast enough to decay to background well within the
335 evolution time of $1.2\ \mu\text{s}$ used in the liposome DEER measurements. The decays do not show
336 oscillations, as is frequently observed for spin pairs with narrow distance distributions [68-71].
337 As a control to rule out lateral aggregation [69], we attached a single spin-label to residue 37C
338 and did not observe a dipolar evolution (DEER shape) that could indicate a pair with a shorter
339 than $\sim 80\text{\AA}$ separation based on only slightly concave shape of the signal (**Fig. 4E**). The DEER
340 data thus suggest that conspicuous dipolar signals in the doubly labeled proteins result from
341 intramolecular interactions, rather than being caused by intermolecular interactions on
342 membranes.

343

344 Distance distributions could be obtained in the presence of liposomes. The results showed
345 semi-broad distance spreads of ~20-40Å for the 25C/96C pair and ~20-35Å for the 37C/114C
346 pair (**Fig. 4F, 4G**). These distances are comparable but do not exactly match the simulated
347 distances using the AlphaFold and RoseTTAFold structure predictions that have only modest
348 confidence levels (**Fig. 4A**) [57, 58]. For comparison, an extended alpha helix would result in
349 distances of ~100Å for these two sites. We also checked the spectral shape by recording field-
350 swept echo with pulse separation of 250ns and did not notice any conspicuous broadening that
351 could indicate a shorter range of distances (<15Å). We do however see from continuous wave
352 (CW) ESR of 37C/114C (**Fig. S6**) that there might be a sizeable fraction of spins in the 15-20Å
353 range whose contribution to the distance distribution will be significantly attenuated, since DEER
354 has low sensitivity to distances in this range. The conformations with this distance range
355 correlate well with AlphaFold predictions. The spread of the P(r) to longer distances could
356 originate from the mobility of the C-terminal helix where residue 114C is located (**Fig. 4C**).
357 Taken together, we concluded that the PAT domain does form a folded domain when bound to
358 membranes and this domain is likely mobile with a structure similar but not identical to the
359 AlphaFold and RoseTTAFold predictions.

360

361 **DAG recruits PLIN3 to membrane bilayers and droplets in vitro**

362 To verify a role for the PAT domain in DAG binding, we conducted an independent set of
363 experiments to test if purified PLIN3 with GFP fused to the N-terminus bound DAG enriched
364 membranes using droplet embedded vesicles (DEVs) [7, 35, 45, 72]. DEVs have emerged as a
365 powerful in vitro system to model emerging LDs that bud from membrane bilayers. A major
366 advantage of DEVs is the ability to not only monitor membrane association, but to also examine
367 the protein distribution and preference for droplet monolayers versus membrane bilayers.

368

369 DEVs were generated by adding the neutral lipids TAG or DAG to giant unilamellar vesicles
370 (GUVs) of DOPC that were marked with fluorescent phospholipids (**Fig. 5A**). As observed
371 previously [45, 73], full length PLIN3 was strongly recruited to the monolayer surface of triolein
372 droplets with almost no bilayer signal (**Fig. 5B, 5D**). Addition of diolein (DO-DAG) generated
373 small droplet buds, and full length PLIN3 was recruited equally to the droplet and bilayer surface
374 (**Fig. 5C, 5D**). Residues 1-204 of PLIN3 that contained both the PAT domain and 11-mer
375 repeats behaved nearly identical to full length PLIN3 in both TAG and DAG containing DEVs
376 (**Fig. 5B, 5C and 5E**).

377

378 Next, we tested fragments of the PAT domain and 11-mer repeats using both triolein and diolein
379 DEVs. The 11-mer repeats preferentially bound the droplet surface of triolein DEVs with the
380 magnitude of signal dependent on the length of the 11-mer repeats (**Fig. 5B, 5G and 5I**). In
381 contrast, PAT domain fragments did not bind to the droplet or bilayer surface of triolein DEVs
382 (**Fig. 5B, 5F and 5H**). The PAT domain was recruited to diolein DEVs, and the largest fragment
383 (residues 1-116) bound to both the droplet and bilayer surface with similar magnitudes to full
384 length PLIN3 (**Fig. 5C, 5F and 5H**). The 11-mer repeats also bound to both the droplet and
385 bilayer surface of diolein DEVs, but to a lesser extent (**Fig. 5C, 5G and 5I**). These results are
386 consistent with our previous hypothesis that the PAT domain is larger than previously expected
387 and that this functional PAT domain binds DAG enriched membranes, while the 11-mer repeats
388 can also bind DAG enriched membranes but display a preference for TAG containing droplets
389 over membrane bilayers.

390

391 **DAG accumulation is sufficient to recruit PLIN3 to the ER in cells**

392 DAG has previously been proposed to recruit PLIN3 to the ER in cells by blocking its hydrolysis
393 or acylation or by the exogenous addition of DAG [74]. This is consistent with the current model
394 for LD formation, where DAG accumulates at the site of TAG nucleation on the ER membrane
395 [18, 19, 75], the local high concentration of neutral lipids promotes LD nucleation through seipin
396 [15], and cytoplasmic PLIN3 marks these sites [10, 49]. We sought to test whether DAG
397 accumulation was sufficient for PLIN3 recruitment using an independent system and also
398 assess what fragments of PLIN3 were necessary and sufficient for ER recruitment.

399

400 To best visualize PLIN3 recruitment to ER membranes, we generated intracellular giant ER
401 vesicles (GERVs) by submitting cells to hypotonic medium [72, 76, 77] (**Fig. 6A**). After
402 exchange to hypotonic medium, cells were pretreated with DMSO or the DGAT inhibitors
403 (DGATi), followed by oleic acid to induce TAG or DAG synthesis [77] (**Fig. 6A**). Confocal
404 microscopy was used to visualize cells prior and after exchange to hypotonic medium, and after
405 oleic acid treatment. Imaging was done in the following minutes after the treatments.

406

407 As expected, the majority of subcellular localization of GFP-tagged PLIN3 was cytoplasmic in
408 both normal and hypotonic media without addition of oleic acid (**Fig. 6B, upper panels**), and co-
409 localized with LDs (**Fig. 6D**). Under conditions of DGAT inhibition, PLIN3 co-localized to the
410 outer periphery of GERVs (**Fig. 6B, yellow arrow, 6E and 6F**), which suggests DO-DAG
411 accumulation is sufficient to recruit PLIN3 to ER membrane bilayers.

412

413 In line with our previous results, a construct containing both the PAT domain and 11-mer
414 repeats showed a similar subcellular localization as full length PLIN3 under all conditions (**Fig.**
415 **6C-6F**). This suggests the PAT domain and 11-mer repeats are sufficient for PLIN3 recruitment
416 to both DAG enriched membrane bilayers and TAG containing LDs, which might also contain
417 DAG whose concentration could increase the protein binding level. Interestingly, constructs
418 containing only the PAT domain (residues 1-116) or only the 11-mer repeats (residues 114-204),
419 which bound to DEVs in a DAG-dependent manner, remained cytoplasmic under all conditions
420 (**Fig. 6D, 6E, S7**). Taken together, we concluded that PLIN3 is capable of binding both DAG
421 enriched ER membranes and early LDs, and that the PAT domain and 11-mer repeats are both
422 necessary and synergize to perform these functions in cells.

423

424

425 **DISCUSSION**

426 Here we find that PLIN3 not only binds LDs, but also membrane bilayers enriched in DAG and
427 PA. These results are in line with other studies that revealed PLIN3 binding to DAG [74, 78, 79].
428 In our hands, DAG binding was observed with multiple in vitro systems (e.g. liposomes, DEVs)
429 and DAG was also sufficient for PLIN3 recruitment to the ER in cells. Cellular recruitment to
430 membranes by DAG is consistent with a seminal study that used inhibitors to block DAG
431 hydrolysis or acylation and exogenous DAG to promote ER recruitment of PLIN3 [74].
432 Independent experiments in yeast have also demonstrated that membrane-anchored PLIN3 is
433 sufficient to bind to DAG enriched subdomains in the ER [78, 79]. Here we show that oleate
434 addition in combination with DGAT inhibition is sufficient for the subcellular redistribution of
435 PLIN3 to the ER, which mimics normal the LD biogenesis pathway.

436
437 There are several mechanistic implications of PLIN3 recruitment to DAG enriched membranes.
438 First, this implies that PLIN3 is recruited to sites of LD formation, not only through TAG
439 generation, but also at the initial stages when DAG begins to accumulate. This raises a likely
440 possibility that PLIN3 may play an active role in the early stages of LD formation by stabilizing
441 DAG enriched regions on ER [78], and define sites of LD formation, before or in concomitant
442 with seipin. Once PLIN3 binds to accumulated DAG, it might coat the curved surface of a
443 growing DAG/TAG lens and regulate LD budding, in conjunction with seipin.

444
445 PA is another TAG precursor that is present at sites where LD originate [17] and can bind to
446 seipin [16]. In addition to DAG, it was found to have a significant impact on the recruitment of
447 PLIN3 to membranes in vitro. Thus, it may increase the translocation of PLIN3 to early LD
448 formation sites. These two TAG precursors appear to provide specificity for the association of
449 PLIN3 with membranes. From a curvature standpoint, DAG has a more negative curvature
450 compared to PA and PE, whereas PE has a more negative curvature than PA [80]. This
451 suggests that membrane curvature cannot solely account for the major role of PA in PLIN3
452 membrane binding specificity. However, from a surface charge perspective, PA and PE together
453 may act synergistically by increasing charge of PA on the membrane [46, 81, 82]. In this
454 scenario, PLIN3 recruitment to LD nucleation sites could be enhanced by specific recognition of
455 PA, potentially through the 4-helix bundle. Therefore, PLIN3 membrane association may not
456 only be determined by membrane packing defects, but could also involve selective physical
457 interactions between PLIN3 and DAG or PA. This idea is also supported by a previous study

458 that found that the LD binding properties of PLINs are sensitive to the polar residue composition
459 of their amphipathic helices [83].

460

461 In this study, we attempted to clarify the function and boundaries of the PAT domain. Our HDX-
462 MS results using full length PLIN3 clearly implicate both the PAT domain and 11-mer repeats in
463 membrane binding. In addition, we were able to define a functional PAT domain that
464 encompasses all of the conserved residues within PLINs and is longer than previously
465 suggested. This expanded PLIN3 PAT domain is sufficient to bind DAG enriched membranes,
466 but not LDs. In contrast, the 11-mer repeats display some affinity for DAG enriched membranes
467 and are necessary to bind LD monolayers. Our overall conclusion is that the PAT domain and
468 11-mer repeats serve synergistic functions, as the individual regions are necessary for both LD
469 and DAG recruitment in cells.

470

471 The PAT domain is predicted to adopt a triangular tertiary structure by both AlphaFold and
472 RoseTTAFold. The DEER distance measurements and CW ESR data are not identical to these
473 predictions, but do indicate that when bound to membranes the PAT domain adopts a folded
474 domain. This conclusion is supported by our HDX-MS results that found the peptides within the
475 PAT domain display longer protection times from H-D exchange, which could be due to either a
476 tertiary structure more resistant to unfolding or a longer membrane residency time. We note that
477 the membrane bound PAT domain structure is likely dynamic and additional distance
478 measurements at distinct sites are needed to verify the accuracy of the predicted triangular
479 structures.

480

481 To our knowledge, our finding that the PAT domain of PLIN3 is sufficient to bind DAG
482 represents the first functional role for the PAT domain in any PLIN. This suggests that the highly
483 conserved PAT domain in other PLINs may serve similar or related functions. For example,
484 could the PAT domain be a general sensor for DAG in membrane bilayers? Or could the PAT
485 domain of other PLINs potentially bind to other neutral lipids (e.g. CEs, TAGs, retinol esters)?
486 Given the previously observed differing neutral lipid preference of PLINs [20] and the
487 involvement of the PAT domain in lipid/membrane binding, this now raises the questions if this
488 is due to the PAT domain preference, the 11-mer repeat preference, or the synergistic action of
489 the combined PAT/11-mer repeat units.

490

491 Lastly, our results are consistent with previous studies that found the PLIN3 4-helix bundle does
492 not bind LDs, but other PLINs 4-helix bundles can bind LDs [33]. While the domain boundaries
493 of the 4-helix bundles seem reasonable given structure of mouse PLIN3 [54], the variable
494 membrane binding affinities we observed for the PAT domain and 11-mer repeats does raise
495 the question if stability of 4-helix bundle, and consequently the ability to unfold and bind
496 membranes or LDs in other PLINs may depend on the domain boundaries of specific constructs.
497 Thus, we suggest it is reasonable to revisit the ability of the 4-helix bundles from other PLINs
498 using constructs that can be stably purified in vitro to rule out potential artifacts from the use of
499 unstable 4-helix bundles.

500

501

502 MATERIALS AND METHODS

503 Protein expression and purification

504 The genes encoding PLIN3 constructs were codon-optimized for expression in *Escherichia coli*
505 and cloned into pTHT, which is a derivative of pET28 that contains a TEV cleavable N-terminal
506 6x His tag. For GFP tagged PLIN3 constructs, monomeric superfolder GFP (msfGFP) was
507 inserted between the 6x His tag and the N-terminus of PLIN3. PLIN3 plasmids were
508 transformed into BL21(DE3) RIPL cells and protein expression was induced with 1mM isopropyl
509 β -D-1-thiogalactopyranoside (IPTG) at 37°C for 3h. Cells was harvested by centrifugation at
510 3,320 x g for 20mins and stored at -80°C until use. Cell pellets were resuspended with buffer A
511 containing 500mM NaCl, 20 mM Tris-HCl pH 7.5, 5% glycerol, 5mM 2-mercaptoethanol (BME)
512 and lysed by sonication. Cell lysates were centrifuged at 81,770 x g for 1h at 4°C and the
513 resulting supernatant was incubated with 5mL of Ni-NTA resin for 2h at 4°C prior to loading onto
514 a gravity column. The Ni-NTA resin was washed with buffer B containing 500mM NaCl, 20mM
515 Tris-HCl pH 7.5, 5% glycerol, 5mM BME and 60mM imidazole. Human PLIN3 proteins were
516 eluted with buffer C containing 500mM NaCl, 20mM Tris-HCl pH 7.5, 5% glycerol, 5mM BME
517 and 300mM imidazole. Eluted protein was applied to a HiLoad 26/600 Superdex 200 pg column
518 (GE life sciences) equilibrated with 150mM NaCl, 20mM Tris-HCl pH 7.5, 5% glycerol, and 5mM
519 BME. The average yield of full length PLIN3, PAT/11-mer repeats and 4-helix bundle throughout
520 expression and purification was between 5-10mg from a 1L culture of *Escherichia coli*. The yield
521 of PAT or 11-mer repeats constructs or GFP tagged PLIN3 fragments was ~1mg/L. Protein was
522 analyzed by SDS-PAGE, concentrated using a centrifugal tube (10K MWCO, Pall Corporation),
523 aliquoted and stored at -80°C.

524

525 Lipids

526 The following lipids were purchased from Avanti Polar Lipids: 1,2-dioleoyl-sn-glycero-3-
527 phosphocholine (DOPC, catalog #850375), 1,2-dioleoyl-sn-glycero-3-phosphoethanolamine
528 (DOPE, catalog #850725), 1,2-dioleoyl-sn-glycero-3-phosphate (DOPA, catalog #840875), 1,2-
529 dioleoyl-sn-glycero-3-phospho-L-serine (DOPS, catalog #840035), 1-palmitoyl-2-oleoyl-glycero-
530 3-phosphocholine (POPC, catalog #850457), 1-palmitoyl-2-oleoyl-sn-glycero-3-
531 phosphoethanolamine (POPE, catalog #850757), 1-palmitoyl-2-oleoyl-sn-glycero-3-phosphate
532 (POPA, catalog #840857), 1-palmitoyl-2-oleoyl-sn-glycero-3-phospho-L-serine (POPS, catalog
533 #840034), 1,2-diphytanoyl-sn-glycero-3-phosphocholine (4ME-PC, catalog #850356), 1,2-
534 diphytanoyl-sn-glycero-3-phosphoethanolamine (4ME-PE, catalog #850402), 1,2-diphytanoyl-

535 sn-glycero-3-phosphate (4ME-PA, catalog #850406), 1,2-diphytanoyl-sn-glycero-3-phospho-L-
536 serine (4ME-PS, catalog #850408), 1-palmitoyl-2-oleoyl-sn-glycerol (DAG, catalog #800815), L-
537 α -phosphatidylinositol (Soy PI, catalog #84044), L- α -phosphatidylinositol-4-phosphate (Brain,
538 Porcine (PI(4)P, catalog #840045), N-stearoyl-D-erythro-sphingosine (C18:1 ceramide, catalog
539 #860518). 1,2,3-Trioleoyl Glycerol was purchase from Cayman Chemicals (TAG, catalog
540 #26950).

541

542 **Liposome co-sedimentation assay**

543 To prepare liposomes, lipids were dried under a nitrogen gas stream and dissolved with buffer
544 containing 50mM NaCl and 50mM HEPES pH 8.0 with a total lipid concentration of 2mM, unless
545 otherwise noted. Liposomes were generated by repeated cycles of flash freezing in liquid
546 nitrogen, thawing in 37°C water bath, and vortexing (ref Traïkia et al). Liposomes were
547 characterized using dynamic light scattering and showed uniform distribution for most lipid
548 compositions. Lamellarity analysis of liposomes was not carried out, but liposomes likely
549 contained a mixture of multi-lamellar vesicles and unilamellar vesicles. For liposome co-
550 sedimentation assays, 20 μ L of 12 μ M purified protein was incubated with 40 μ L of 2 mM
551 liposomes for 40mins at 23°C. Protein fractions bound to liposomes were isolated by
552 centrifugation at 100,000 x g for 70mins at 4°C and analyzed by SDS-PAGE.

553

554 **Circular Dichroism**

555 Circular dichroism (CD) spectra of purified PLIN3 full length and its constructs were measured
556 on Spectropolarimeter (Jasco, J-715). 0.12~0.24mg/ml of protein was incubated with 1~2mM
557 liposomes containing 4ME-PC/PE/PA for 40mins prior to measurement. Liposomes/protein
558 mixture was prepared in the buffer containing 20mM Tris pH 7.5 and 150mM NaCl. CD spectra
559 was measured between 190nm and 260nm in increments of 1nm, with a bandwidth of 50nm
560 and an averaging time of 1min at 25°C. 10 iterations of spectra were averaged and was
561 reported into a mDeg, which was converted to molar ellipticity ($m^{\circ}M/(10^{\circ}L^{\circ}C)$) of which unit is
562 expressed in degree $cm^2 dmol^{-1}$. Molar ellipticity of each protein fragments in the absence or
563 presence were plotted using GraphPad prism software. Comparisons of spectra in the presence
564 and the absence of liposome were assessed using unpaired *t* test with $p < 0.05$ of statistical
565 significance.

566

567 **Artificial lipid droplet flotation assay**

568 Artificial lipid droplets (ALDs) were prepared by mixing phospholipids and triacylglycerols
569 (TAGs). Di-oleoyl phospholipids were dried under a nitrogen gas stream. Dried lipids were
570 resuspended with lipid droplet flotation assay buffer containing 50mM NaCl and 50mM HEPES
571 pH 8.0 and TAGs in the molar ratio of 2:5. ALDs were formed by repeating the cycles of vortex
572 for 10sec and rest for 10sec. ALDs were further vortexed before use for the assay. 100 μ L of
573 ALDs were mixed with 5 μ L of human PLIN3 and 105 μ L of lipid flotation assay buffer to give a
574 final concentration of 5 μ M protein and 1.5mM phospholipids. The average diameters of different
575 ALDs were measured by dynamic light scattering (DLS). The concentration of ALDs were
576 determined by optical density at 600nm. The mixture of human PLIN3 and ALDs was incubated
577 for 1h at 23°C. To generate a sucrose gradient, 140 μ L of a 75% sucrose solution was added to
578 210 μ L of the protein-ALD mixture to give a final concentration of 30% sucrose. The resulting
579 mixture (320 μ L) was transferred to an ultra-centrifuge tube. 260 μ L of a 25% sucrose solution
580 was applied on top of 30% sucrose/protein/ALDs mixture. Lastly, 60 μ L of lipid flotation assay
581 buffer was laid on the top. ALDs were floated by centrifugation at 76,000 x g for 3h at 20°C with
582 sucrose gradient of 30% (bottom), 25% (middle), and 0% (top). Three fractions of 100 μ L from
583 the top, 260 μ L from the middle and 280 μ L from the bottom were collected and analyzed by
584 SDS-PAGE.

585

586 **Hydrogen-Deuterium Exchange Mass Spectrometry (HDX-MS)**

587 *Sample preparation*

588 HDX reactions for PLIN3 deuterium pulse were conducted in a final reaction volume of 10 μ L
589 with a final concentration 2.12 μ M PLIN3. Exchange was carried out in triplicate for a single time
590 point (3 sec at 0 °C). Hydrogen deuterium exchange was initiated by the addition of 9 μ L of D2O
591 buffer solution (20mM HEPES pH 7.5, 100mM NaCl) to 1 μ L of protein, to give a final
592 concentration of 84.9% D2O. Exchange was terminated by the addition of 60 μ L acidic quench
593 buffer at a final concentration 0.6M guanidine-HCl and 0.9% formic acid. Samples were
594 immediately frozen in liquid nitrogen at -80°C. Fully deuterated samples were generated by first
595 denaturing the protein in 3M guanidine for 1h at 20°C. Following denaturing, 9 μ L of D2O buffer
596 was added to the 1 μ L of denatured protein and allowed to incubate for 10mins at 20°C before
597 quenching with 0.6M guanidine-HCl and 0.9% formic acid. Samples were immediately frozen in
598 liquid nitrogen at -80°C, and all timepoints were created and run in triplicate.

599

600 HDX reactions comparing PLIN3 in the presence of PA liposomes (60mol% 4ME-PC, 20mol%
601 4ME-PE, 20mol% 4ME-PA) were conducted in a final reaction volume of 10 μ L with a final
602 protein concentration of 3 μ M and final liposome concentration of 1mM. Protein and liposomes
603 were preincubated together for 2mins at 20°C before the addition of 7 μ L D2O buffer solution
604 (50mM HEPES pH 8.0, 50mM NaCl) for a final concentration of 63% D2O. Exchange was
605 carried out for 3sec, 30sec, 300sec and 3000sec, and exchange was terminated by the addition
606 of 60 μ L acidic quench buffer at a final concentration 0.6M guanidine-HCl and 0.9% formic acid.
607 Samples were immediately frozen in liquid nitrogen at -80°C, and all timepoints were created
608 and run in triplicate.

609
610 HDX reactions comparing PLIN3 in the presence of two different liposomes (60mol% DOPC,
611 20mol% DOPE, 20mol% DAG liposomes and 80mol% 4ME-PC, 20mol% 4ME-PE liposomes)
612 were conducted in a final reaction volume of 10 μ L with a final protein concentration of 3 μ M and
613 final liposome concentration of 500 μ M. Protein and liposomes were preincubated together for
614 2mins at 20°C before the addition of 8 μ L D2O buffer solution (50mM HEPES pH 8.0, 50mM
615 NaCl) for a final concentration of 72% D2O. Exchange was carried out for 3sec, 30sec, 300sec
616 and 3000sec, and exchange was terminated by the addition of 60 μ L acidic quench buffer at a
617 final concentration 0.6M guanidine-HCl and 0.9% formic acid. Samples were immediately frozen
618 in liquid nitrogen at -80°C, and all timepoints were created and run in triplicate.

619
620 *Protein digestion and MS/MS data collection*

621 Protein samples were rapidly thawed and injected onto an integrated fluidics system containing
622 a HDx-3 PAL liquid handling robot and climate-controlled (2°C) chromatography system (LEAP
623 Technologies), a Dionex Ultimate 3000 UHPLC system, as well as an Impact HD QTOF Mass
624 spectrometer (Bruker). The protein was run over either one (at 10°C) or two (at 10°C and 2°C)
625 immobilized pepsin columns (Trajan; ProDx protease column, 2.1mm x 30mm PDX.PP01-F32)
626 at 200 μ L/min for 3mins. The resulting peptides were collected and desalted on a C18 trap
627 column (Acquity UPLC BEH C18 1.7mm column (2.1 x 5mm); Waters 186003975). The trap
628 was subsequently eluted in line with an ACQUITY 1.7 μ m particle, 100 x 1mm² C18 UPLC
629 column (Waters), using a gradient of 3-35% B (Buffer A 0.1% formic acid; Buffer B 100%
630 acetonitrile) over 11mins immediately followed by a gradient of 35-80% over 5mins. Mass
631 spectrometry experiments acquired over a mass range from 150 to 2200m/z using an
632 electrospray ionization source operated at a temperature of 200°C and a spray voltage of 4.5kV.

633

634 *Peptide identification*

635 Peptides were identified from the non-deuterated samples of PLIN3 using data-dependent
636 acquisition following tandem MS/MS experiments (0.5sec precursor scan from 150-2000m/z;
637 twelve 0.25sec fragment scans from 150-2000m/z). MS/MS datasets were analyzed using
638 PEAKS7 (PEAKS), and peptide identification was carried out by using a false discovery based
639 approach, with a threshold set to 1% using a database of known contaminants found in Sf9 and
640 *E. coli* cells [84]. The search parameters were set with a precursor tolerance of 20ppm,
641 fragment mass error 0.02 Da, charge states from 1-8, leading to a selection criterion of peptides
642 that had $-10\log P$ scores of 22.8 for the pulse experiment and 20.9 for the liposome experiment.

643

644 *Mass Analysis of Peptide Centroids and Measurement of Deuterium Incorporation*

645 HD-Examiner Software (Sierra Analytics) was used to automatically calculate the level of
646 deuterium incorporation into each peptide. All peptides were manually inspected for correct
647 charge state, correct retention time, appropriate selection of isotopic distribution, etc.
648 Deuteration levels were calculated using the centroid of the experimental isotope clusters.
649 Results are presented as relative levels of deuterium incorporation, with the only correction
650 being applied correcting for the deuterium oxide percentage of the buffer utilized in the
651 exchange (63% and 72%). For the experiment with a fully deuterated sample, corrections for
652 back exchange were made by dividing the pulse %D value by the fully deuterated %D value and
653 multiplying by 100. The raw %D incorporation for the fully deuterated sample is included in the
654 source data, with the average back exchange being 33%, and ranging from 10-60%.
655 Differences in exchange in a peptide were considered significant if they met all three of the
656 following criteria: $\geq 5\%$ change in exchange and ≥ 0.4 Da difference in exchange. The raw HDX
657 data are shown in two different formats. Samples were only compared within a single
658 experiment and were never compared to experiments completed at a different time with a
659 different final D₂O level. The data analysis statistics for all HDX-MS experiments are in
660 Supplemental Table 1 according to the guidelines of [85]. The mass spectrometry proteomics
661 data have been deposited to the ProteomeXchange Consortium via the PRIDE partner
662 repository with the dataset identifier PXD025717 [86].

663

664 **Dynamic light scattering**

665 The size of liposomes was measured by dynamic light scattering (Brookhaven Instruments
666 NanoBrook Omni), with or without full length PLIN3. Liposomes were prepared in the buffer
667 containing 50mM HEPES pH 8.0 and 50mM NaCl by repeating the freeze/thaw cycles to
668 prevent multilamellar vesicle formation. Each protein construct was incubated with liposomes in
669 1:200 of molar ratio at 25°C for 40mins. DLS was conducted using a scattering angle of 90°,
670 and the liposome/protein mixture was equilibrated for 5mins after loading into the instrument to
671 get a uniform temperature and minimize any loading effects prior to measurement. The number
672 average size distribution (%) was considered as a relative concentration of particles with a
673 certain size. For analysis, measurements with large outlier peaks, which were suspected to be
674 due to the dust particles or aggregated vesicles, were discarded, and three runs that did not
675 contain outlier peaks were used for the data analysis. The mode of the distribution (e.g., the size
676 having the highest peak in the number average size distribution) was chosen from each of these
677 three measurements and averaged to obtain the reported average diameter. A representative
678 size distribution is shown for each sample.

679

680 **Site-directed spin-labeling**

681 Recombinant PLIN3 cysteine-substituted proteins were purified using Ni-NTA resin in a buffer
682 500mM NaCl, 20mM Tris pH 7.5, 5% glycerol and eluted in a buffer of 500mM NaCl, 20mM Tris
683 pH 7.5, 5% Glycerol, 300mM imidazole. Elution was spin-labeled with 1µg/mL (S-(1-oxyl-
684 2,2,5,5-tetramethyl-2,5-dihydro-1H-pyrrol-3-yl) methyl methanesulfonothioate), MTSL, (Santa
685 Cruz Biotech) dissolved in acetonitrile at 4°C overnight. The spin-labeled proteins were further
686 purified by HiLoad 26/600 Superdex 200 pg column (GE life sciences) in a buffer of 150mM
687 NaCl, 20mM Tris pH 7.5 to remove unreacted spin labels.

688

689 **Sample preparations for DEER spectroscopy**

690 Protein samples in solutions were prepared at ca. 40-60µM concentrations in 20mM Tris at pH
691 7.5, 150mM NaCl, and 40% glycerol. Liposome samples containing 10µM protein and 3.33 mM
692 lipid were prepared by mixing 30µM protein stocks with 5mM liposome solutions using 1 to 2
693 aliquots followed by 30mins incubation at room temperature. The liposomes were freshly
694 prepared by rehydration of lyophilized 80/20 mol% 4ME-PC/PE followed by seven freeze/thaw
695 cycles. Freshly-prepared 20µL of spin-labeled samples were loaded into 1.8mm inner diameter
696 Pyrex sample tubes (Wilma-LabGlass), frozen by plunging in liquid nitrogen, and stored in
697 liquid nitrogen for PDS measurements.

698

699 DEER data collection and analysis

700 PDS DEER measurements were performed at 60K with a home-built Ku band pulse ESR
701 spectrometer operating around 17.3GHz [64, 87]. A four-pulse DEER sequence [88] was
702 employed using for spin-echo detection $\pi/2$ - and π -pulses with respective widths of 16 and 32ns,
703 the π -pulse for pumping was 16ns. The detection frequency matched the peak at the low-field
704 spectral edge, while pumping was performed at a lower by 70MHz frequency, corresponding to
705 the central maximum. A 32-step phase cycle [89] was applied to suppress unwanted
706 contributions to the signal. Nuclear electron spin-echo envelope modulation (ESEEM) caused
707 by surrounding protons was suppressed using the data from four measurements. In this method
708 the initial pulse separations and the start of detection were advanced by 9.5ns in subsequent
709 measurements, i.e. by the quarter period of the 26.2MHz nuclear Zeeman frequency for protons
710 at 0.615T corresponding to the working frequency. The four signal traces were summed to
711 achieve deep suppression of nuclear ESEEM, [90].

712

713 The solution samples had phase memory times, T_m 's, of about 2.5 μ s, so the data could be
714 recorded up to 3 μ s evolution time (t_m). Such evolution times did not provide sufficient decay of
715 the dipolar coherence to the background level, providing however clear indication of
716 unstructured nature of the protein in solution. Any residual secondary structure could be probed
717 by using multiple labeling sites, however other techniques did not encourage this undertaking.
718 For solutions the DEER data were acquired in less than 12h. Faster phase relaxation times
719 ($\sim 1\mu$ s) and low spin concentrations in liposome samples required signal averaging for ~ 24 h to
720 facilitate good reconstruction by Tikhonov regularization. [91, 92]

721

722 For liposomes, time domain DEER data, $V(t)$, were recorded and preprocessed using standard
723 approaches [62, 65, 88, 93] before their reconstruction into distance distributions, $P(r)$'s. The
724 first step is to remove signal decay caused by intermolecular dipole-dipole couplings, followed
725 by subtracting the residual background from the spins whose partner was not flipped by the
726 pump or missing. This was done, as usual, by fitting the latter points (about a half of the record)
727 of $\ln[V(t)]$ to a low-order polynomial, usually a straight line for solutions (and often for liposomes),
728 extrapolating it to zero time, and subtracting out from $\ln[V(t)]$; so that the antilog yields $u(t) = d(t)$
729 $+ 1$. Here $d(t)$ is the dipolar evolution representing part. Once $u(t)$ is normalized as $u(t)/u(0)$, it
730 serves as a typical form of DEER data presentation, while $v(t)=(u(t)-1)/u(0)$, gives background-
731 free "dipolar" data to be converted to a distance distribution between spins in pairs. We used L-
732 curve Tikhonov regularization [91] for distance reconstruction. The Tikhonov regularization utility

733 allowed selection of either the signal or its derivatives in the Tikhonov functional and selection of
734 the regularization parameter. The latter increases $P(r)$ smoothness at the expense of
735 introducing some broadening.

736
737 Dipolar signal amplitude (“modulation depth”) is given by $v(0)$. This would be accurate to the
738 extent the background or $V(\infty)$, the asymptotic value of $V(t)$, is known. This depth, tabulated by
739 calculations for typical pulse sequence setup and verified in numerous experiments, is a
740 measure of a fraction of spins in pairs or oligomers [69, 94, 95]. It is thus useful in estimate of
741 spin-labeling efficiency and protein concentration.

742
743 **Cell culture**
744 Cos7 cells were maintained in Dulbecco’s modified Eagle’s medium (DMEM) supplemented with
745 10% heat inactivated fetal bovine serum (Life Technologies), 4.5gL^{-1} D-glucose, 0.1gL^{-1} sodium
746 pyruvate (Life Technologies) and 1% penicillin-streptomycin (Life Technologies). The cells were
747 cultured at 37°C under a 5% CO_2 atmosphere.

748
749 **Transfection**
750 When indicated, Cos7 cells (60–70% confluence) plated into a 35mm cell-culture Mattek dishes
751 (with a glass coverslip at the bottom), (MatTek Corp. Ashland, MA). were transfected with $3\mu\text{g}$ of
752 plasmid DNA/ml using Polyethylenimine HCl MAX (Polysciences) following the manufacturer’s
753 instructions. For co-expressions, RFP-KDEL or GFP-Plin3 constructs in equal concentrations
754 ($1.5\text{--}2\mu\text{g}$ for each one) were transfected to cells 24h prior observation.

755
756 **Giant unilamellar vesicles, GUVs**
757 GUVs were prepared by electroformation following the protocol described in [96]. Phospholipids,
758 dioleoyl phosphatidylcholine (PC) (70%) and dioleoyl phosphatidylethanolamine (PE) (29%),
759 Rhodamine-DOPE 1% (w/w)), were purchased from Avanti Polar Lipids. The lipid mixture, in
760 chloroform at 0.5mM , was dried on an indium tin oxide (ITO)-coated glass plate. The lipid film
761 was desiccated for 1h. The chamber was sealed with another ITO- coated glass plate. The
762 lipids were then rehydrated with a sucrose solution (275mOsm). Electroformation was done
763 using 100Hz AC voltage at 1.0 to 1.4Vpp and maintained for at least 1h.

764
765 **Droplet-embedded vesicles (DEVs) preparation**

766 Artificial LDs (aLDs) were prepared in HKM buffer: 50mM HEPES, 120mM Kacetate, and 1mM
767 MgCl₂ (in Milli-Q water) at pH 7.4 and 275±15mOsm. To do so, 5µL of the lipid oil solution
768 (triolein or diacylglycerol purchased from Sigma) was added to 45mL of HKM buffer and the
769 mixture was sonicated as described in [97]. The resulting emulsion was then mixed with GUVs
770 for five minutes under rotator to generate DEVs [97]. DEVs were then placed on a glass
771 coverslip pretreated with 10%(w/w) BSA and washed three times with buffer.

772

773 **Protein binding to DEVs**

774 For the protein binding experiments, 50µL HKM were deposited on the BSA-treated glass, 30µL
775 of the DEV solution added and 1.5µL purified PLIN3 or PLIN3 fragments added (in the case of
776 107-204 and 1-106 fragments, 3µL were added). The final protein concentration in the solution
777 was between 1µM to 4µM depending on the protein. For quantifications, 10-15 DEVs were
778 considered and the signal on the droplet and bilayer was determined by Fiji, via drawing 5-10
779 points-thick line profiles.

780

781 **Neutral lipid synthesis induction**

782 Wherever relevant, cells were exposed for 1h to 350µM oleic acid (OA) coupled to bovine serum
783 albumin (BSA) (0.2% weight/volume) to induce neutral lipids' synthesis. LipidTox DeepRed
784 (Thermo Fischer), was used to visualize lipid droplets or membranes enriched in neutral lipids.

785

786 **Giant Intra-Cellular ER vesicle experiments**

787 For GERV experiments, Cos7 cells were first transfected for 24h with the indicated eGFP
788 plasmids and RFP-KDEL. The culture media of the cells was next replaced by a hypotonic
789 culture media (DMEM:H₂O, 1:20). The cells were then incubated at 37°C, 5% CO₂ for 5mins, to
790 induce GERVs, and then they were visualized. Neutral lipids' synthesis was triggered by the
791 addition of OA and Z-stacks imaging of different entire cells was performed before and 15mins
792 after OA administration, as described in [77]. For the DGAT1 (Sigma, PF-04620110) and
793 DGAT2 (Sigma, PF-06424439) inhibitors used in Cos7, the dilution applied was 1/1000 for a
794 final concentration of 3µg/mL. In the GERV protocol, the inhibitors were added to the cell
795 medium before cell transfection or during the hypotonic solution addition. The signal of PLIN3 or
796 fragments thereof was quantified for tens of GERVs by depicting the mean signal on the GERVs
797 to which was subtracted the bulk cytosolic signal; this resulted signal was normalized to the
798 cytosolic signal.

799

800 **Structure prediction by AlphaFold and RoseTTAFold**

801 Structure prediction of PLIN3 was carried out by AlphaFold and RoseTTAFold. Two different
802 confidence values were generated (pLDDT from AlphaFold and rmsd from RoseTTAFold).
803 These values were converted using PHENIX to get relative confidence level from two softwares,
804 AlphaFold and RoseTTAFold [98].

805

806

807

808 **REFERENCES**

809

- 810 1. Thiam, A.R., R.V. Farese, Jr., and T.C. Walther, *The biophysics and cell biology of lipid*
811 *droplets*. Nat Rev Mol Cell Biol, 2013. **14**(12): p. 775-86.
- 812 2. Rubin, C.S., et al., *Development of hormone receptors and hormonal responsiveness in*
813 *vitro. Insulin receptors and insulin sensitivity in the preadipocyte and adipocyte forms of*
814 *3T3-L1 cells*. J Biol Chem, 1978. **253**(20): p. 7570-8.
- 815 3. Gibbons, G.F., K. Islam, and R.J. Pease, *Mobilisation of triacylglycerol stores*. Biochim
816 Biophys Acta, 2000. **1483**(1): p. 37-57.
- 817 4. Olzmann, J.A. and P. Carvalho, *Dynamics and functions of lipid droplets*. Nat Rev Mol Cell
818 Biol, 2019. **20**(3): p. 137-155.
- 819 5. Valm, A.M., et al., *Applying systems-level spectral imaging and analysis to reveal the*
820 *organelle interactome*. Nature, 2017. **546**(7656): p. 162-167.
- 821 6. Miyanari, Y., et al., *The lipid droplet is an important organelle for hepatitis C virus*
822 *production*. Nat Cell Biol, 2007. **9**(9): p. 1089-97.
- 823 7. Ben M'barek, K., et al., *ER Membrane Phospholipids and Surface Tension Control Cellular*
824 *Lipid Droplet Formation*. Dev Cell, 2017. **41**(6): p. 591-604 e7.
- 825 8. Choudhary, V., et al., *A conserved family of proteins facilitates nascent lipid droplet*
826 *budding from the ER*. J Cell Biol, 2015. **211**(2): p. 261-71.
- 827 9. Thiam, A.R. and L. Foret, *The physics of lipid droplet nucleation, growth and budding*.
828 Biochim Biophys Acta, 2016. **1861**(8 Pt A): p. 715-22.
- 829 10. Chung, J., et al., *LDAF1 and Seipin Form a Lipid Droplet Assembly Complex*. Dev Cell,
830 2019. **51**(5): p. 551-563 e7.
- 831 11. Gao, M., et al., *The biogenesis of lipid droplets: Lipids take center stage*. Prog Lipid Res,
832 2019. **75**: p. 100989.
- 833 12. Chorlay, A., et al., *Membrane Asymmetry Imposes Directionality on Lipid Droplet*
834 *Emergence from the ER*. Dev Cell, 2019. **50**(1): p. 25-42 e7.
- 835 13. Wang, H., et al., *Seipin is required for converting nascent to mature lipid droplets*. Elife,
836 2016. **5**.
- 837 14. Salo, V.T., et al., *Seipin regulates ER-lipid droplet contacts and cargo delivery*. EMBO J,
838 2016. **35**(24): p. 2699-2716.
- 839 15. Zoni, V., et al., *Pre-existing bilayer stresses modulate triglyceride accumulation in the ER*
840 *versus lipid droplets*. Elife, 2021. **10**.

- 841 16. Yan, R., et al., *Human SEIPIN Binds Anionic Phospholipids*. Dev Cell, 2018. **47**(2): p. 248-
842 256 e4.
- 843 17. Guyard, V., et al., *ORP5 and ORP8 orchestrate lipid droplet biogenesis and maintenance*
844 *at ER-mitochondria contact sites*. J Cell Biol, 2022. **221**(9).
- 845 18. Choudhary, V., et al., *Seipin and Nem1 establish discrete ER subdomains to initiate yeast*
846 *lipid droplet biogenesis*. J Cell Biol, 2020. **219**(7).
- 847 19. Choudhary, V., et al., *Architecture of Lipid Droplets in Endoplasmic Reticulum Is*
848 *Determined by Phospholipid Intrinsic Curvature*. Curr Biol, 2018. **28**(6): p. 915-926 e9.
- 849 20. Hsieh, K., et al., *Perilipin family members preferentially sequester to either*
850 *triacylglycerol-specific or cholesteryl-ester-specific intracellular lipid storage droplets*. J
851 Cell Sci, 2012. **125**(Pt 17): p. 4067-76.
- 852 21. Wolins, N.E., D.L. Brasaemle, and P.E. Bickel, *A proposed model of fat packaging by*
853 *exchangeable lipid droplet proteins*. FEBS Lett, 2006. **580**(23): p. 5484-91.
- 854 22. Brasaemle, D.L., *Thematic review series: adipocyte biology. The perilipin family of*
855 *structural lipid droplet proteins: stabilization of lipid droplets and control of lipolysis*. J
856 Lipid Res, 2007. **48**(12): p. 2547-59.
- 857 23. Greenberg, A.S., et al., *Perilipin, a major hormonally regulated adipocyte-specific*
858 *phosphoprotein associated with the periphery of lipid storage droplets*. J Biol Chem,
859 1991. **266**(17): p. 11341-6.
- 860 24. Jiang, H.P. and G. Serrero, *Isolation and characterization of a full-length cDNA coding for*
861 *an adipose differentiation-related protein*. Proc Natl Acad Sci U S A, 1992. **89**(17): p.
862 7856-60.
- 863 25. Diaz, E. and S.R. Pfeffer, *TIP47: a cargo selection device for mannose 6-phosphate*
864 *receptor trafficking*. Cell, 1998. **93**(3): p. 433-43.
- 865 26. Wolins, N.E., et al., *Adipocyte protein S3-12 coats nascent lipid droplets*. J Biol Chem,
866 2003. **278**(39): p. 37713-21.
- 867 27. Sztalryd, C. and D.L. Brasaemle, *The perilipin family of lipid droplet proteins: Gatekeepers*
868 *of intracellular lipolysis*. Biochim Biophys Acta Mol Cell Biol Lipids, 2017. **1862**(10 Pt B): p.
869 1221-1232.
- 870 28. Wilson, M.H., S.C. Ekker, and S.A. Farber, *Imaging cytoplasmic lipid droplets in vivo with*
871 *fluorescent perilipin 2 and perilipin 3 knock-in zebrafish*. Elife, 2021. **10**.
- 872 29. Bulankina, A.V., et al., *TIP47 functions in the biogenesis of lipid droplets*. J Cell Biol, 2009.
873 **185**(4): p. 641-55.
- 874 30. Rowe, E.R., et al., *Conserved Amphipathic Helices Mediate Lipid Droplet Targeting of*
875 *Perilipins 1-3*. J Biol Chem, 2016. **291**(13): p. 6664-78.
- 876 31. Copic, A., et al., *A giant amphipathic helix from a perilipin that is adapted for coating*
877 *lipid droplets*. Nat Commun, 2018. **9**(1): p. 1332.
- 878 32. Mirheydari, M., et al., *Insertion of perilipin 3 into a glycerol(phospho)lipid monolayer*
879 *depends on lipid headgroup and acyl chain species*. J Lipid Res, 2016. **57**(8): p. 1465-76.
- 880 33. Ajjaji, D., et al., *Dual binding motifs underpin the hierarchical association of perilipins1-3*
881 *with lipid droplets*. Mol Biol Cell, 2019. **30**(5): p. 703-716.
- 882 34. Bigay, J. and B. Antonny, *Curvature, lipid packing, and electrostatics of membrane*
883 *organelles: defining cellular territories in determining specificity*. Dev Cell, 2012. **23**(5): p.
884 886-95.

- 885 35. Chorlay, A. and A.R. Thiam, *Neutral lipids regulate amphipathic helix affinity for model*
886 *lipid droplets*. J Cell Biol, 2020. **219**(4).
- 887 36. Prevost, C., et al., *Mechanism and Determinants of Amphipathic Helix-Containing*
888 *Protein Targeting to Lipid Droplets*. Dev Cell, 2018. **44**(1): p. 73-86 e4.
- 889 37. Vamparys, L., et al., *Conical lipids in flat bilayers induce packing defects similar to that*
890 *induced by positive curvature*. Biophys J, 2013. **104**(3): p. 585-93.
- 891 38. Zhukovsky, M.A., et al., *Phosphatidic acid in membrane rearrangements*. FEBS Lett, 2019.
892 **593**(17): p. 2428-2451.
- 893 39. Vanni, S., et al., *A sub-nanometre view of how membrane curvature and composition*
894 *modulate lipid packing and protein recruitment*. Nat Commun, 2014. **5**: p. 4916.
- 895 40. Fujimoto, Y., et al., *Long-chain fatty acids induce lipid droplet formation in a cultured*
896 *human hepatocyte in a manner dependent of Acyl-CoA synthetase*. Biol Pharm Bull, 2006.
897 **29**(11): p. 2174-80.
- 898 41. Harayama, T. and H. Riezman, *Understanding the diversity of membrane lipid*
899 *composition*. Nat Rev Mol Cell Biol, 2018. **19**(5): p. 281-296.
- 900 42. Radhakrishnan, A., et al., *Switch-like control of SREBP-2 transport triggered by small*
901 *changes in ER cholesterol: a delicate balance*. Cell Metab, 2008. **8**(6): p. 512-21.
- 902 43. Listenberger, L., et al., *Decreasing Phosphatidylcholine on the Surface of the Lipid*
903 *Droplet Correlates with Altered Protein Binding and Steatosis*. Cells, 2018. **7**(12).
- 904 44. Titus, A.R., et al., *The C-Terminus of Perilipin 3 Shows Distinct Lipid Binding at*
905 *Phospholipid-Oil-Aqueous Interfaces*. Membranes (Basel), 2021. **11**(4).
- 906 45. Caillon, L., et al., *Triacylglycerols sequester monotopic membrane proteins to lipid*
907 *droplets*. Nat Commun, 2020. **11**(1): p. 3944.
- 908 46. Putta, P., et al., *Phosphatidic acid binding proteins display differential binding as a*
909 *function of membrane curvature stress and chemical properties*. Biochim Biophys Acta,
910 2016. **1858**(11): p. 2709-2716.
- 911 47. Chorlay, A., L. Foret, and A.R. Thiam, *Origin of gradients in lipid density and surface*
912 *tension between connected lipid droplet and bilayer*. Biophys J, 2021. **120**(24): p. 5491-
913 5503.
- 914 48. Garten, M., et al., *Methyl-branched lipids promote the membrane adsorption of alpha-*
915 *synuclein by enhancing shallow lipid-packing defects*. Phys Chem Chem Phys, 2015.
916 **17**(24): p. 15589-97.
- 917 49. Wolins, N.E., et al., *S3-12, Adipophilin, and TIP47 package lipid in adipocytes*. J Biol Chem,
918 2005. **280**(19): p. 19146-55.
- 919 50. Englander, S.W. and N.R. Kallenbach, *Hydrogen exchange and structural dynamics of*
920 *proteins and nucleic acids*. Q Rev Biophys, 1983. **16**(4): p. 521-655.
- 921 51. Skinner, J.J., et al., *Protein hydrogen exchange: testing current models*. Protein Sci, 2012.
922 **21**(7): p. 987-95.
- 923 52. Balasubramaniam, D. and E.A. Komives, *Hydrogen-exchange mass spectrometry for the*
924 *study of intrinsic disorder in proteins*. Biochim Biophys Acta, 2013. **1834**(6): p. 1202-9.
- 925 53. Vadas, O., et al., *Using Hydrogen-Deuterium Exchange Mass Spectrometry to Examine*
926 *Protein-Membrane Interactions*. Methods Enzymol, 2017. **583**: p. 143-172.
- 927 54. Hickenbottom, S.J., et al., *Structure of a lipid droplet protein; the PAT family member*
928 *TIP47*. Structure, 2004. **12**(7): p. 1199-207.

- 929 55. Hynson, R.M., et al., *Solution structure studies of monomeric human TIP47/perilipin-3*
930 *reveal a highly extended conformation*. *Proteins*, 2012. **80**(8): p. 2046-55.
- 931 56. Weis, D.D., et al., *Identification and characterization of EX1 kinetics in H/D exchange*
932 *mass spectrometry by peak width analysis*. *J Am Soc Mass Spectrom*, 2006. **17**(11): p.
933 1498-1509.
- 934 57. Jumper, J., et al., *Highly accurate protein structure prediction with AlphaFold*. *Nature*,
935 2021. **596**(7873): p. 583-589.
- 936 58. Baek, M., et al., *Accurate prediction of protein structures and interactions using a three-*
937 *track neural network*. *Science*, 2021. **373**(6557): p. 871-876.
- 938 59. Najt, C.P., et al., *Structural and functional assessment of perilipin 2 lipid binding*
939 *domain(s)*. *Biochemistry*, 2014. **53**(45): p. 7051-66.
- 940 60. Milov, A., K. Salikhov, and M. Shirov, *Application of ELDOR in electron-spin echo for*
941 *paramagnetic center space distribution in solids*. *Fizika Tverdogo Tela*, 1981. **23**(4): p.
942 975-982.
- 943 61. Pannier, M., et al., *Characterization of Ionic Clusters in Different Ionically Functionalized*
944 *Diblock Copolymers by CW EPR and Four-Pulse Double Electron–Electron Resonance*.
945 *Macromolecules*, 2001. **34**(16): p. 5555-5560.
- 946 62. Borbat, P.P. and J.H. Freed, *Pulse Dipolar Electron Spin Resonance: Distance*
947 *Measurements*, in *Structural Information from Spin-Labels and Intrinsic Paramagnetic*
948 *Centres in the Biosciences*, C.R. Timmel and J.R. Harmer, Editors. 2014. p. 1-82.
- 949 63. Borbat, P.P. and J.H. Freed, *Dipolar Spectroscopy - Single-resonance Methods*. *Emagres*,
950 2017. **6**(4): p. 465-493.
- 951 64. Borbat, P.P., E.R. Georgieva, and J.H. Freed, *Improved Sensitivity for Long-Distance*
952 *Measurements in Biomolecules: Five-Pulse Double Electron–Electron Resonance*. *Journal*
953 *of Physical Chemistry Letters*, 2013. **4**(1): p. 170-175.
- 954 65. Jeschke, G., *DEER Distance Measurements on Proteins*, in *Annual Review of Physical*
955 *Chemistry, Vol 63*, M.A. Johnson and T.J. Martinez, Editors. 2012. p. 419-446.
- 956 66. Bahrenberg, T., et al., *rDEER: A Modified DEER Sequence for Distance Measurements*
957 *Using Shaped Pulses*. *Magnetochemistry*, 2019. **5**(1).
- 958 67. Sung, Y.H. and D. Eliezer, *Residual structure, backbone dynamics, and interactions within*
959 *the synuclein family*. *J Mol Biol*, 2007. **372**(3): p. 689-707.
- 960 68. Tong, J.S., et al., *A scissors mechanism for stimulation of SNARE-mediated lipid mixing by*
961 *cholesterol*. *Proceedings of the National Academy of Sciences of the United States of*
962 *America*, 2009. **106**(13): p. 5141-5146.
- 963 69. Georgieva, E.R., et al., *Mechanism of influenza A M2 transmembrane domain assembly*
964 *in lipid membranes*. *Sci Rep*, 2015. **5**: p. 11757.
- 965 70. Borbat, P., et al., *Inter-helix distances in lysophospholipid micelle-bound alpha-synuclein*
966 *from pulsed ESR measurements*. *Journal of the American Chemical Society*, 2006.
967 **128**(31): p. 10004-10005.
- 968 71. Jeschke, G., et al., *Interresidual distance determination by four-pulse double electron-*
969 *electron resonance in an integral membrane protein: the Na⁺/proline transporter PutP*
970 *of Escherichia coli*. *Biophysical Journal*, 2004. **86**(4): p. 2551-2557.
- 971 72. Santinho, A., et al., *Membrane Curvature Catalyzes Lipid Droplet Assembly*. *Curr Biol*,
972 2020. **30**(13): p. 2481-2494 e6.

- 973 73. Ma, X., et al., *Validating an artificial organelle: Studies of lipid droplet-specific proteins*
974 *on adiposome platform*. iScience, 2021. **24**(8): p. 102834.
- 975 74. Skinner, J.R., et al., *Diacylglycerol enrichment of endoplasmic reticulum or lipid droplets*
976 *recruits perilipin 3/TIP47 during lipid storage and mobilization*. J Biol Chem, 2009.
977 **284**(45): p. 30941-8.
- 978 75. Joshi, A.S., et al., *Lipid droplet and peroxisome biogenesis occur at the same ER*
979 *subdomains*. Nat Commun, 2018. **9**(1): p. 2940.
- 980 76. King, C., et al., *ER membranes exhibit phase behavior at sites of organelle contact*. Proc
981 Natl Acad Sci U S A, 2020. **117**(13): p. 7225-7235.
- 982 77. Ajjaji, D., et al., *Hepatitis C virus core protein uses triacylglycerols to fold onto the*
983 *endoplasmic reticulum membrane*. Traffic, 2022. **23**(1): p. 63-80.
- 984 78. Khaddaj, R. and R. Schneiter, *Perilipin 3 promotes the formation of membrane domains*
985 *enriched in diacylglycerol and lipid droplet biogenesis proteins*. bioRxiv, 2022: p.
986 2022.09.14.507979.
- 987 79. Jacquier, N., et al., *Expression of oleosin and perilipins in yeast promotes formation of*
988 *lipid droplets from the endoplasmic reticulum*. J Cell Sci, 2013. **126**(Pt 22): p. 5198-209.
- 989 80. Zanghellini, J., F. Wodlei, and H.H. von Grunberg, *Phospholipid demixing and the birth of*
990 *a lipid droplet*. J Theor Biol, 2010. **264**(3): p. 952-61.
- 991 81. Kooijman, E.E., et al., *An electrostatic/hydrogen bond switch as the basis for the specific*
992 *interaction of phosphatidic acid with proteins*. J Biol Chem, 2007. **282**(15): p. 11356-64.
- 993 82. Mengistu, D.H., E.E. Kooijman, and S. May, *Ionization properties of mixed lipid*
994 *membranes: a Gouy-Chapman model of the electrostatic-hydrogen bond switch*. Biochim
995 Biophys Acta, 2011. **1808**(8): p. 1985-92.
- 996 83. Gimenez-Andres, M., et al., *Exceptional stability of a perilipin on lipid droplets depends*
997 *on its polar residues, suggesting multimeric assembly*. Elife, 2021. **10**.
- 998 84. Dobbs, J.M., M.L. Jenkins, and J.E. Burke, *Escherichia coli and Sf9 Contaminant*
999 *Databases to Increase Efficiency of Tandem Mass Spectrometry Peptide Identification in*
1000 *Structural Mass Spectrometry Experiments*. J Am Soc Mass Spectrom, 2020. **31**(10): p.
1001 2202-2209.
- 1002 85. Masson, G.R., et al., *Recommendations for performing, interpreting and reporting*
1003 *hydrogen deuterium exchange mass spectrometry (HDX-MS) experiments*. Nat Methods,
1004 2019. **16**(7): p. 595-602.
- 1005 86. Perez-Riverol, Y., et al., *The PRIDE database and related tools and resources in 2019:*
1006 *improving support for quantification data*. Nucleic Acids Res, 2019. **47**(D1): p. D442-
1007 D450.
- 1008 87. Borbat, P.P., R.H. Crepeau, and J.H. Freed, *Multifrequency two-dimensional Fourier*
1009 *transform ESR: an X/Ku-band spectrometer*. J Magn Reson, 1997. **127**(2): p. 155-67.
- 1010 88. Jeschke, G. and Y. Polyhach, *Distance measurements on spin-labelled*
1011 *biomacromolecules by pulsed electron paramagnetic resonance*. Physical Chemistry
1012 Chemical Physics, 2007. **9**(16): p. 1895-1910.
- 1013 89. Gamliel, D. and J.H. Freed, *THEORY OF 2-DIMENSIONAL ESR WITH NUCLEAR*
1014 *MODULATION*. Journal of Magnetic Resonance, 1990. **89**(1): p. 60-93.
- 1015 90. Tang, S.G., et al., *Structural basis for activation, assembly and membrane binding of*
1016 *ESCRT-III Snf7 filaments*. Elife, 2015. **4**.

- 1017 91. Chiang, Y.W., P.P. Borbat, and J.H. Freed, *The determination of pair distance*
1018 *distributions by pulsed ESR using Tikhonov regularization*. Journal of Magnetic
1019 Resonance, 2005. **172**(2): p. 279-295.
- 1020 92. Chiang, Y.W., P.P. Borbat, and J.H. Freed, *Maximum entropy: a complement to Tikhonov*
1021 *regularization for determination of pair distance distributions by pulsed ESR*. Journal of
1022 magnetic resonance (San Diego, Calif.: 1997), 2005a. **177**(2): p. 184-196.
- 1023 93. Borbat, P.P. and J.H. Freed, *Measuring distances by pulsed dipolar ESR spectroscopy:*
1024 *spin-labeled histidine kinases*. Methods Enzymol, 2007. **423**: p. 52-116.
- 1025 94. Bode, B.E., et al., *Counting the monomers in nanometer-sized oligomers by pulsed*
1026 *electron - Electron double resonance*. Journal of the American Chemical Society, 2007.
1027 **129**(21): p. 6736-6745.
- 1028 95. Milov, A.D., A.B. Ponomarev, and Y.D. Tsvetkov, *Modulation beats of signal of double*
1029 *electron-electron resonance in spin echo for biradical systems* Journal of Structural
1030 Chemistry, 1984. **25**(5): p. 710-713.
- 1031 96. Thiam, A.R., et al., *COPI buds 60-nm lipid droplets from reconstituted water-*
1032 *phospholipid-triacylglyceride interfaces, suggesting a tension clamp function*. Proc Natl
1033 Acad Sci U S A, 2013. **110**(33): p. 13244-9.
- 1034 97. Chorlay, A., A. Santinho, and A.R. Thiam, *Making Droplet-Embedded Vesicles to Model*
1035 *Cellular Lipid Droplets*. STAR Protoc, 2020. **1**(3): p. 100116.
- 1036 98. Oeffner, R.D., et al., *Putting AlphaFold models to work with*
1037 *phenix.process_predicted_model and ISOLDE*. Acta Crystallogr D Struct Biol, 2022. **78**(Pt
1038 11): p. 1303-1314.
- 1039 99. Kokorin, A.I., *Nitroxides - Theory, Experiment and Applications*. 2012, Rijeka: IntechOpen.
1040 448.
- 1041 100. Rabenstein, M.D. and Y.K. Shin, *Determination of the distance between two spin labels*
1042 *attached to a macromolecule*. Proc Natl Acad Sci U S A, 1995. **92**(18): p. 8239-43.
1043
1044
1045

1046 **Acknowledgements**

1047
1048 This work was supported by in part by the NIGMS (R35GM128666, MVA), the Sloan Research
1049 Foundation (MVA), the Natural Science and Engineering Research Council of Canada
1050 (Discovery Grant 2020-04241, JEB) with salary support from the Michael Smith Foundation for
1051 Health Research (Scholar award 17868, JEB), the ANR (18-CE11-0012-01-MOBIL, CE11-0032-
1052 02-LIPRODYN and 21-CE13-0014-LIPDROPER, ART), and the NSF (CBET 1903189, SB and
1053 DGE 1922639, SR). ESR study, conducted at ACERT, was supported by NIH/NIGMS grants
1054 1R24GM146107 and P41GM103521.

1055
1056
1057 **Author contributions**

1058
1059 YMC generated constructs for E. coli and mammalian cell expression, purified all proteins,
1060 conducted liposome sedimentation, artificial lipid droplet binding assays, CD, DLS, prepared
1061 figures, and wrote the initial draft. DA conducted all DEV and cell culture experiments. KDF,
1062 MLJ, and BEM setup, analyzed, and/or prepared figures and text from the HDX-MS data. PPB
1063 designed, acquired, and analyzed all PDS-ESR data. JEB, ART, JHF and MVA supervised the
1064 work and provided funding support.

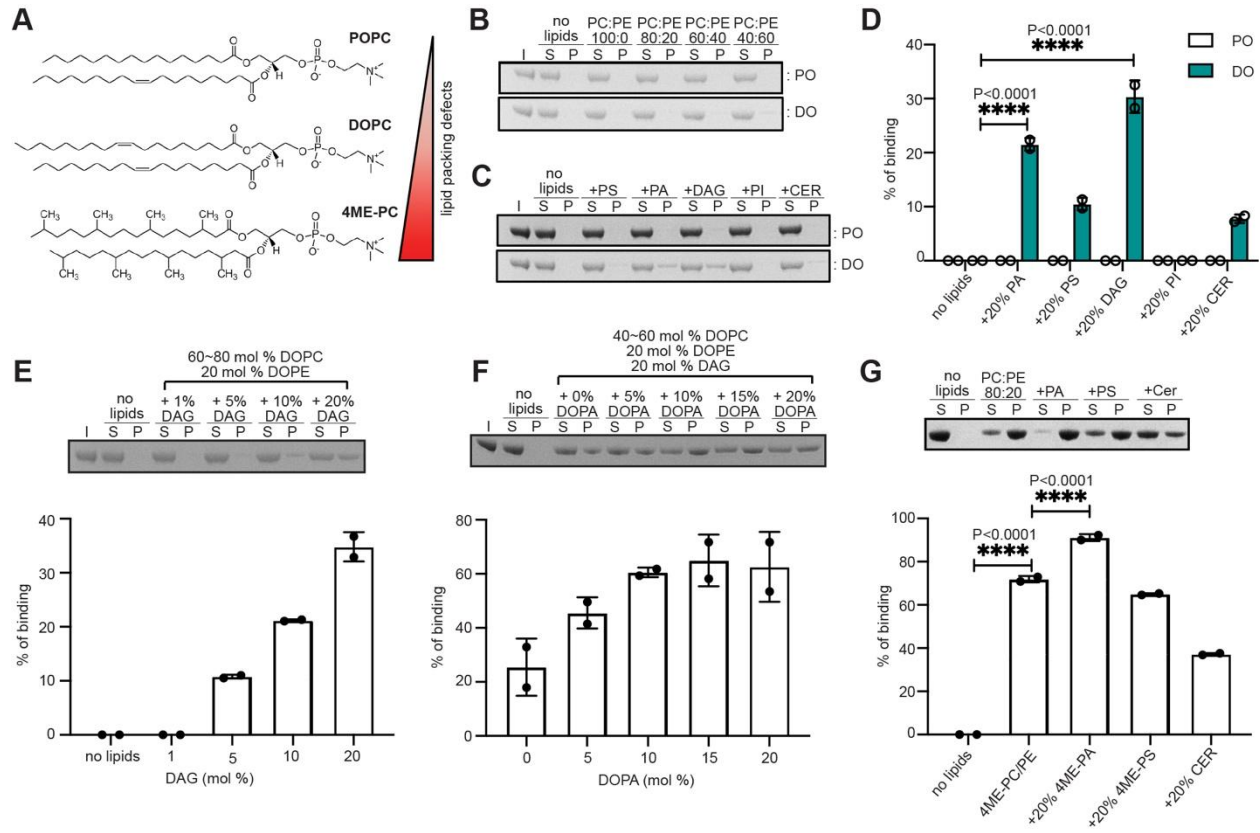
1065
1066 **Competing Interest Statement**

1067
1068 JEB reports personal fees from Scorpion Therapeutics and Olema Oncology; and research
1069 grants from Novartis.

1070
1071
1072
1073
1074
1075
1076

1077
1078

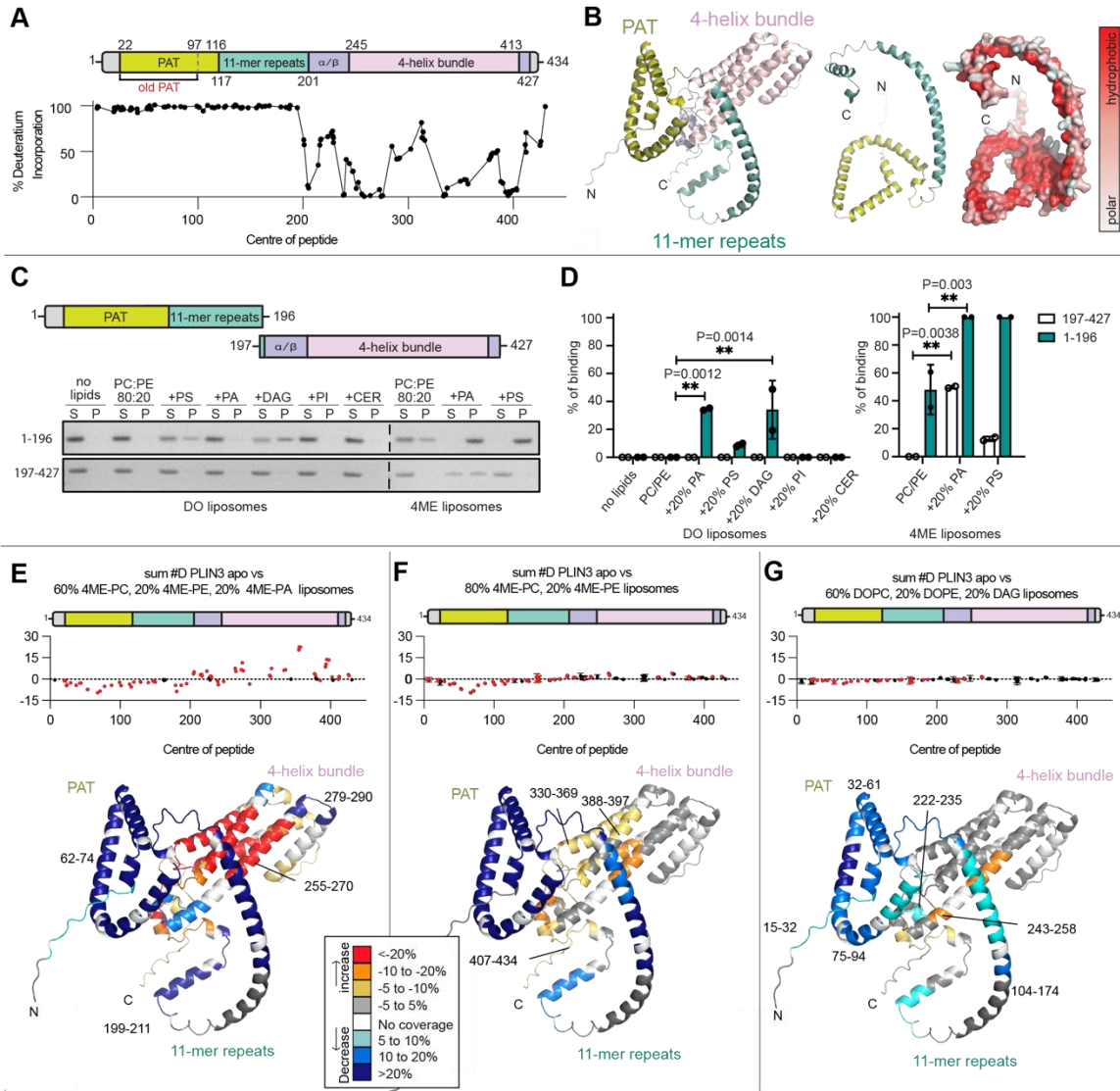
Figures and Figure Legends



1079
1080
1081
1082
1083
1084
1085
1086
1087
1088
1089
1090
1091
1092
1093
1094
1095
1096
1097
1098
1099
1100
1101

Figure 1. Triglyceride precursors DAG and PA recruit PLIN3 to membrane bilayers

A) Structures of representative phospholipids used in this study.
B) SDS-PAGE analysis of human PLIN3 liposome sedimentation assay on the either palmitoyl-oleoyl (PO)-liposomes or di-oleoyl (DO)-liposomes in different ratio of PC to PE. Lane S (supernatant) and P (pellet) represent unbound and bound human PLIN3 to liposomes.
C) SDS-PAGE analysis of human PLIN3 recruitment to liposomes enriched with 20 mol% of the additional lipids PS, PA, DAG, PI and ceramide.
D) Quantification of PLIN3 recruitment to liposomes in different lipid compositions (n=2). Statistical analysis was performed using two-way ANOVA (****, p<0.0001).
E) SDS-PAGE analysis of human PLIN3 recruitment to DO-liposomes using different amounts of DAG. DOPE concentration was held constant at 20mol% and DOPC was adjusted between 60 and 80mol% to maintain total phospholipid concentration. Bar graph shows addition of DAG increases PLIN3 binding.
F) SDS-PAGE analysis of human PLIN3 recruitment to DO-liposomes enriched with different amount of DOPA. The amounts of DOPE and DAG were kept constant at 20mol%. DOPC concentration was adjusted between 40 and 60mol% to maintain total phospholipid concentration. Bar graph shows addition of DOPA further increases PLIN3 binding.
G) SDS-PAGE analysis of human PLIN3 recruitment to 4ME liposomes enriched with 20 mol% of the additional lipids 4ME-PA, 4ME-PS, ceramide. 4ME-PC and 4ME-PE concentrations ranged between 60 ~80mol% and 20mol%, respectively. Statistical analysis for quantification of liposome binding was performed using ordinary one-way ANOVA with Tukey's multiple comparison test (n=2, ****, p<0.0001)



1102
 1103
 1104
 1105
 1106
 1107
 1108
 1109
 1110
 1111
 1112
 1113
 1114
 1115
 1116
 1117
 1118

Figure 2. HDX-MS analysis of PLIN3 membrane binding

A) Absolute percentage of deuterium incorporation after 3sec deuterium exposure of PLIN3 at 1°C in the absence of liposomes. Each point represents a single peptide, with them being graphed on the x-axis according to their central residue. A domain architecture of human PLIN3 was drawn to match the scale of x-axis of HDX-MS. N-terminal PAT domain (mustard) and 11-mer repeats (cyan) have no detectable secondary structure in the absence of liposomes.

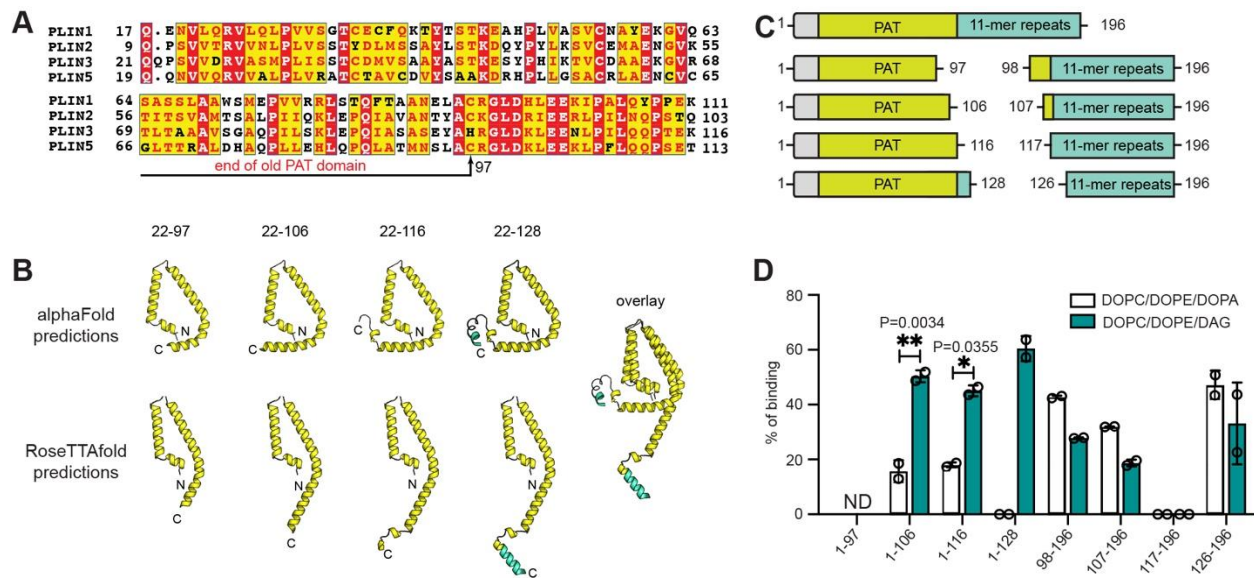
B) A predicted 3D structure of human PLIN3 (UniProt: O60664) by AlphaFold (Left). The surface of PAT domain and 11-mer repeats were shown according to the hydrophobicity (Right).

C) SDS-PAGE and **D)** quantitative analysis of PAT/11-mer repeats and 4-helix bundle liposome binding. DO and 4ME-liposomes were prepared in the same way as Figure 1C and 1D. Statistical analysis for quantification of liposome binding was performed using two-way ANOVA with Tukey's multiple comparison test (n=2).

E-G) Quantitative analysis of deuterium exchange differences of human PLIN3 in the presence of liposomes. The sum of the difference in the # of incorporated deuterons is shown for the absence and the presence of liposomes over all timepoints. The N-terminus composed of

1119 PAT/11-mer repeats was significantly protected from deuterium exchange (defined as > 5%
1120 change in exchange, > 0.4 Da mass difference in exchange, a *p*-value < 0.01 using a two-tailed
1121 Student's *t*-test). Each point represents an individual peptide, with those colored in red having a
1122 significant difference, with error bars showing standard deviation (n=3). Liposomes were
1123 generated with **(E)** 60mol% 4ME-PC, 20mol% 4ME-PE and 20mol% 4ME-PA, **(F)** 80mol% 4ME-
1124 PC, 20mol% 4ME-PE or **(G)** 60mol% DOPC, 20mol% DOPE and 20mol% DAG. A map of
1125 deuterium exchange rate according to all peptides throughout the entire PLIN3 was generated
1126 based on the AlphaFold predicted PLIN3 structure and color coded according to the legend. The
1127 full set of peptides is shown in the source data.

1128
1129
1130
1131
1132
1133
1134
1135
1136
1137
1138
1139
1140
1141
1142
1143
1144
1145
1146
1147
1148
1149
1150
1151
1152
1153
1154
1155
1156
1157
1158
1159
1160
1161
1162
1163
1164
1165



1166
 1167
 1168
 1169
 1170
 1171
 1172
 1173
 1174
 1175
 1176
 1177
 1178

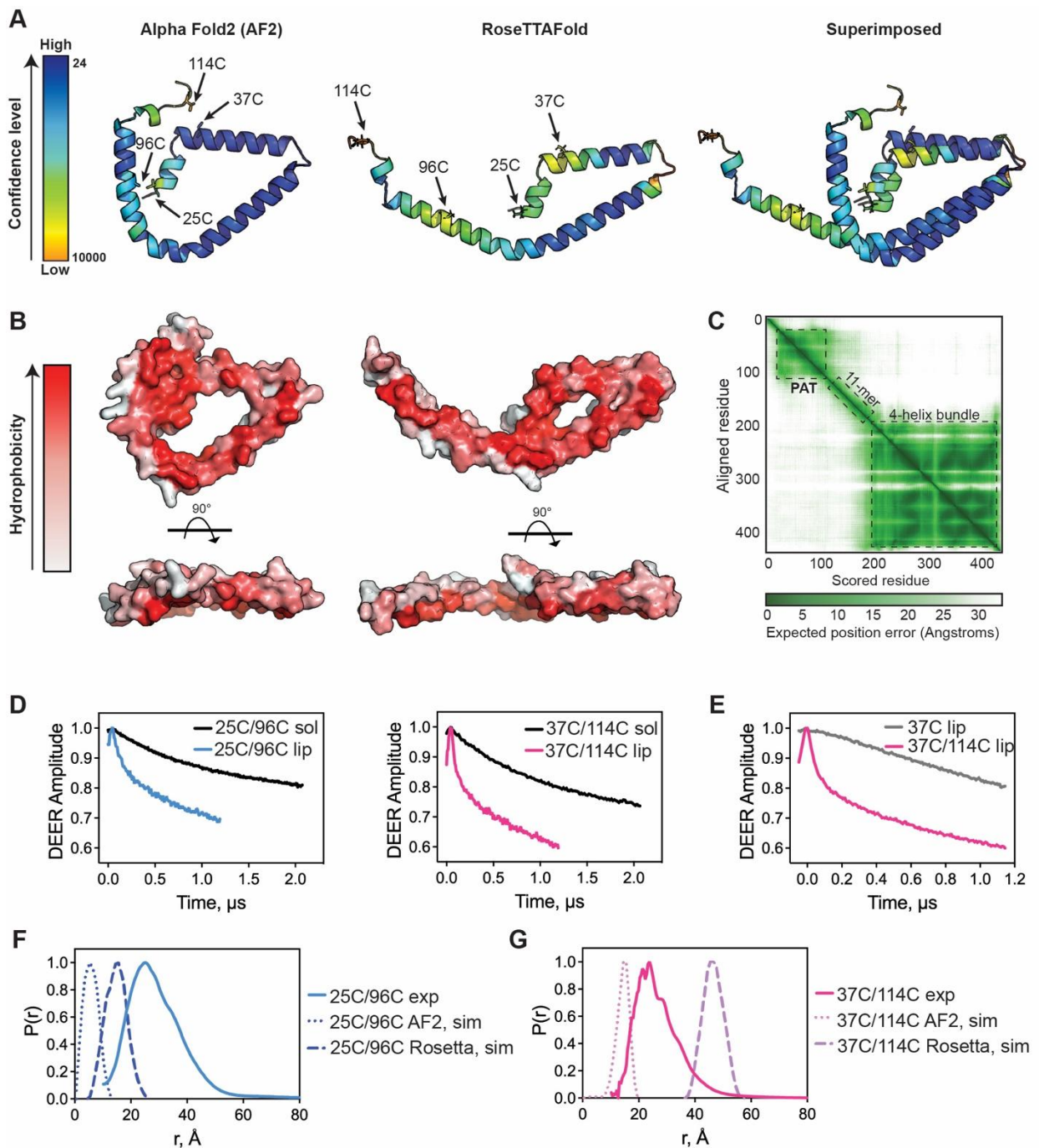
Figure 3. An expanded PAT domain binds DAG enriched membranes

A) Multiple sequence alignment of the N-terminus of human PLIN 1 (UniProt: O60240), PLIN2 UniProt: Q99541), PLIN3 (UniProt: O60664), and PLIN5 (UniProt: Q00G26). The previously suggested PAT domain (residues 1-97) is indicated with black arrow.

B) Putative PAT domain triangular structures predicted by both AlphaFold and RoseTTAFold.

C) Schematic of PAT domain constructs and the counterpart 11-mer repeats constructs.

D) Quantitative analysis of liposome recruitment for various PAT domain and 11-mer repeats constructs. Statistical analysis for quantification of liposome binding was performed using two-way ANOVA with Tukey’s multiple comparison test (n=2).



1179
1180

1181 **Figure 4. Membrane-induced conformational rearrangements are consistent with a PAT**
1182 **domain tertiary structure**

1183 **A)** Cartoon representation of the PAT domain structure predicted by AlphaFold2 and
1184 RoseTTAFold with relative confidence levels shown. The positions of the spin-labeled residues
1185 are indicated with arrows.

1186 **B)** The hydrophobic surface of predicted PAT domain are depicted. The hydrophobic face of the
1187 helices is facing towards the reader.

1188 **C)** The PAE (Predicted Aligned Error) value of AlphaFold2 for full length PLIN3 was plotted by
1189 ChimeraX and shown as an interactive 2D plot (bottom, right panel).

1190 **D)** Time domain signals from DEER spectroscopy of double-labeled 25C/96C (left) and
1191 37C/114C (right) in solution (sol) and on liposomes (lip).
1192 **E)** Time domain signals from DEER spectroscopy of double-labeled 37C/114C and single-
1193 labeled 37C proteins on liposomes.
1194 **F, G)** Distance distributions from DEER spectroscopy of **(E)** 25C/96C and **(F)** 37C/114C
1195 determined experimentally (exp) and from MtsslWizard simulations using the AlphaFold2 (AF2,
1196 sim) and RoseTTAFold (Rosetta, sim) predicted structures.
1197
1198
1199
1200
1201
1202
1203
1204
1205
1206
1207
1208
1209
1210
1211
1212
1213
1214
1215
1216
1217
1218
1219
1220
1221
1222
1223
1224
1225

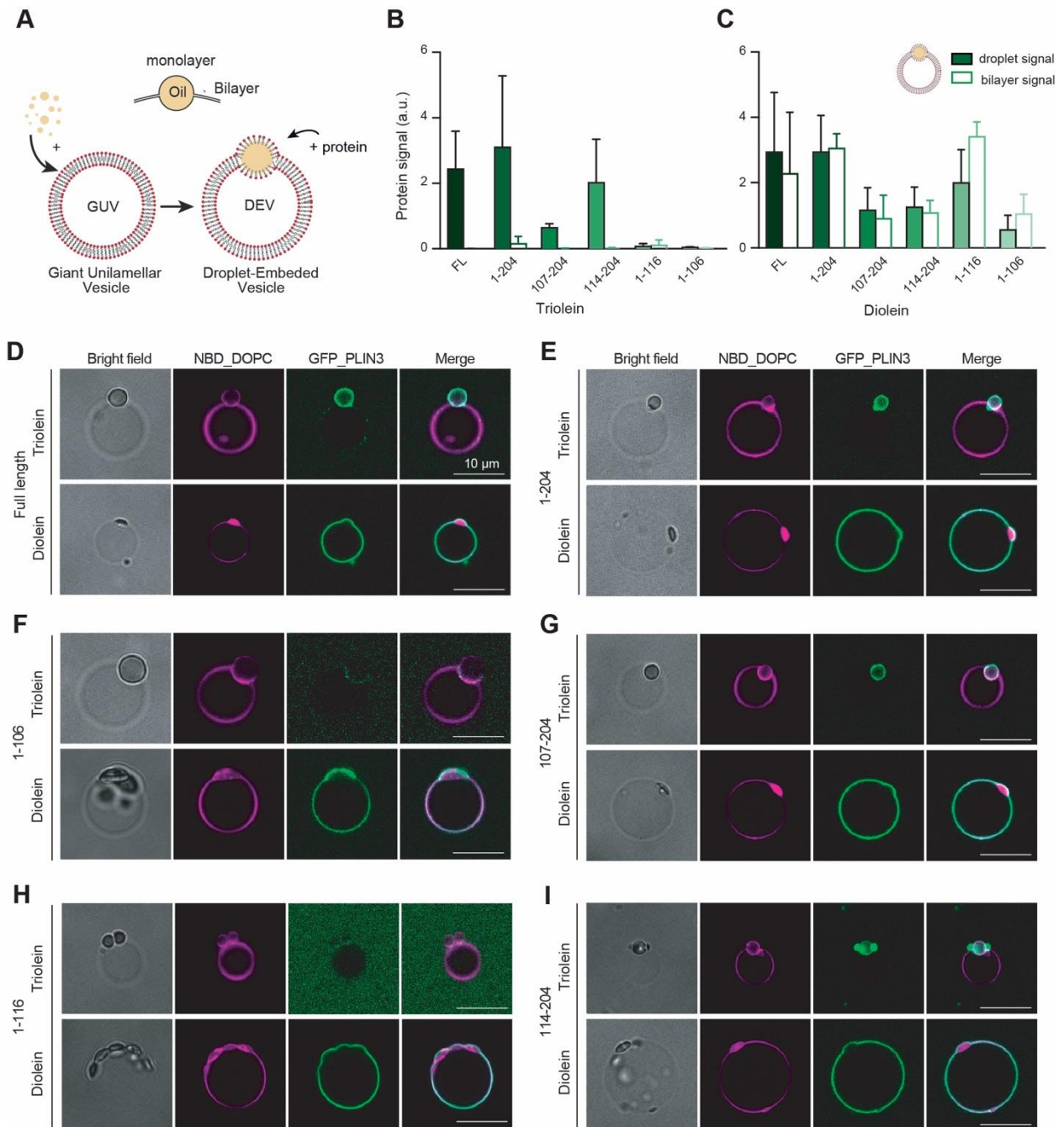


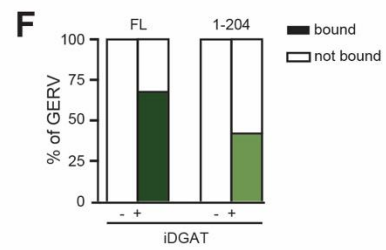
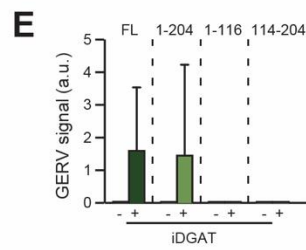
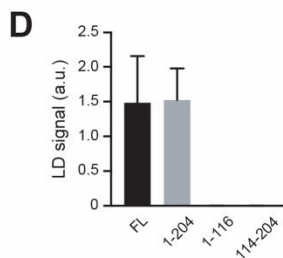
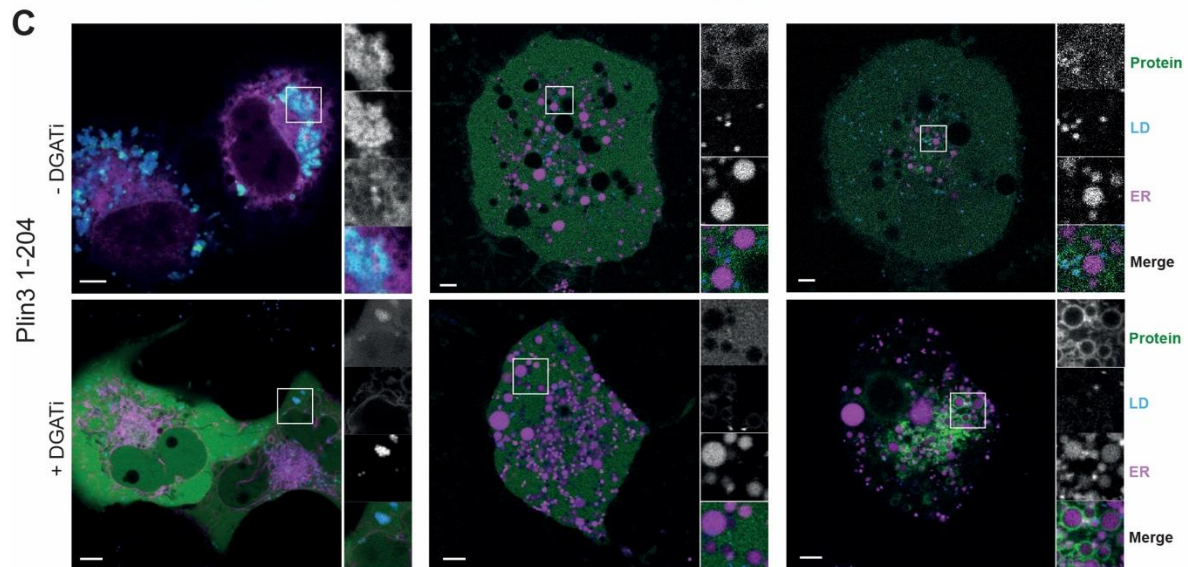
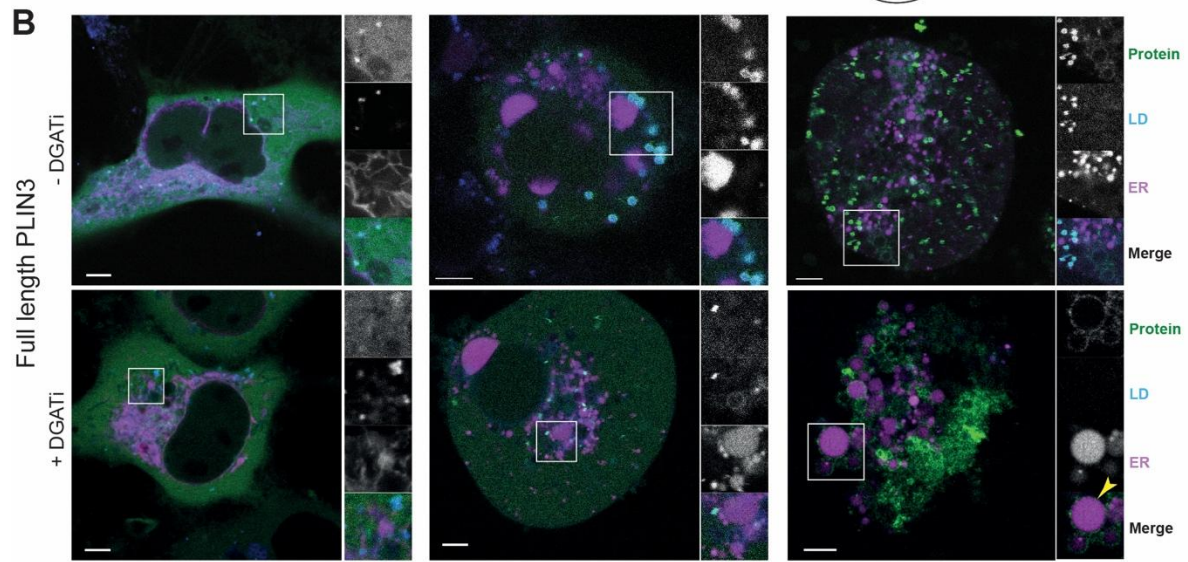
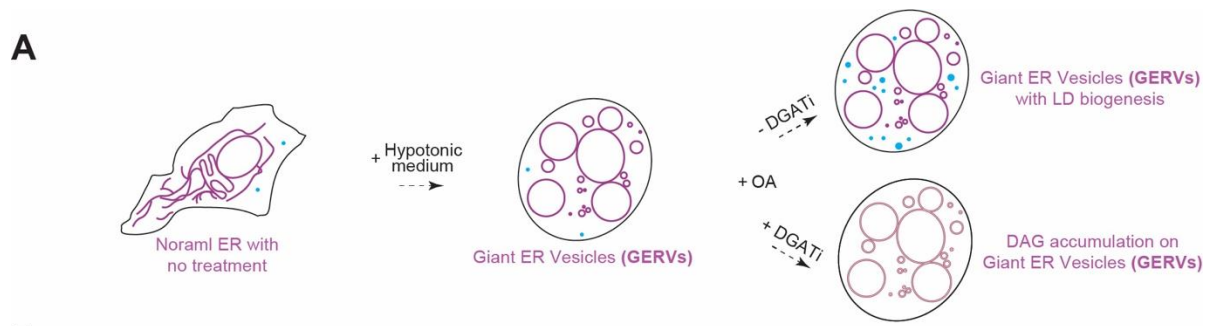
Figure 5. DAG recruits PLIN3 to membrane bilayers and LD droplets in vitro

A) A diagram of generation of DEVs by mixing oils and giant unilamellar vesicles (GUVs).

B, C) Quantification of the recruitment of GFP tagged PLIN3 constructs to droplet embedded vesicles (DEVs) containing (B) triolein or (C) Diolein. Statistical analysis was done with a Mann–Whitney non-parametric test. $P < 0.01$ for all proteins. Three different experiments were performed and 10 to 15 DEVs quantified for each experiment.

D-I) Fluorescent microscopic images of N-terminal GFP tagged full length and PLIN3 constructs (green) comprised of PAT domain and 11-mer repeats to (DEVs) (magenta) that are generated with fluorescent labeled phospholipids and oils. F) and H) Recruitment of PAT domain constructs. Almost no recruitment of PAT domain constructs in the presence of Triolein. G) and I) Recruitment of 11-mer repeats constructs.

1226
1227
1228
1229
1230
1231
1232
1233
1234
1235
1236
1237



1239 **Figure 6. Both PAT domain and 11-mer repeats are necessary for PLIN3 recruitment to**
1240 **DAG enriched ER membranes in Cos7 cells**

1241 **A)** A diagram of treatment of Giant ER Vesicle formation and treatment of oleic acid and DGATi
1242 to induce DAG accumulation on the ER in Cos7 cells.

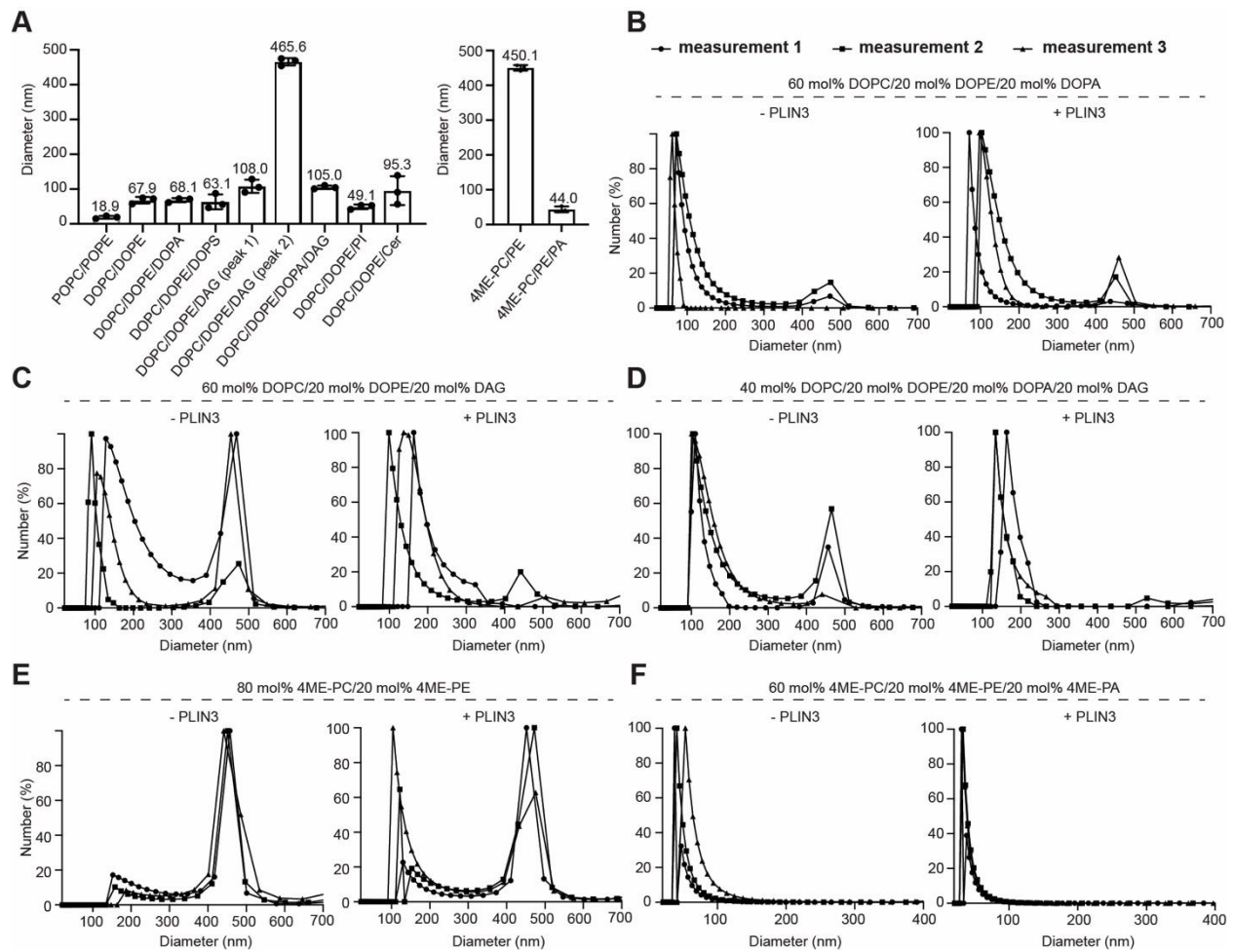
1243 **B, C)** Subcellular localization of GFP tagged full length PLIN3 and PAT/11-mer repeats (1-204)
1244 were visualized in green in Cos7 cells under fluorescent microscope ZEISS LSM800 Airyscan.
1245 ER was visualized with ER specific marker RFP-KDEL in magenta. Lipid droplets were labeled
1246 with LipidTox Deepred to stain neutral lipids in cyan. After treated with hypotonic medium, cells
1247 were supplemented with oleate in the presence or absence of DGAT1/2 inhibitors. Each
1248 experiment was performed more than 3 times.

1249 **D)** Quantification of the amount of various PLIN3 constructs on LDs

1250 **E)** Quantification of the amount of various PLIN3 constructs on GERV after oleate treatment in
1251 the presence and the absence of DGAT1/2 inhibitors.

1252 **F)** % of GERV that are covered with full length PLIN3 or PAT/11-mer repeats construct (1-204)
1253 after oleate treatment in the presence and the absence of DGAT1/2 inhibitors.

1254
1255
1256
1257
1258
1259
1260
1261
1262
1263
1264
1265
1266
1267
1268
1269
1270
1271
1272
1273
1274
1275
1276
1277
1278
1279
1280
1281
1282
1283
1284
1285
1286
1287
1288

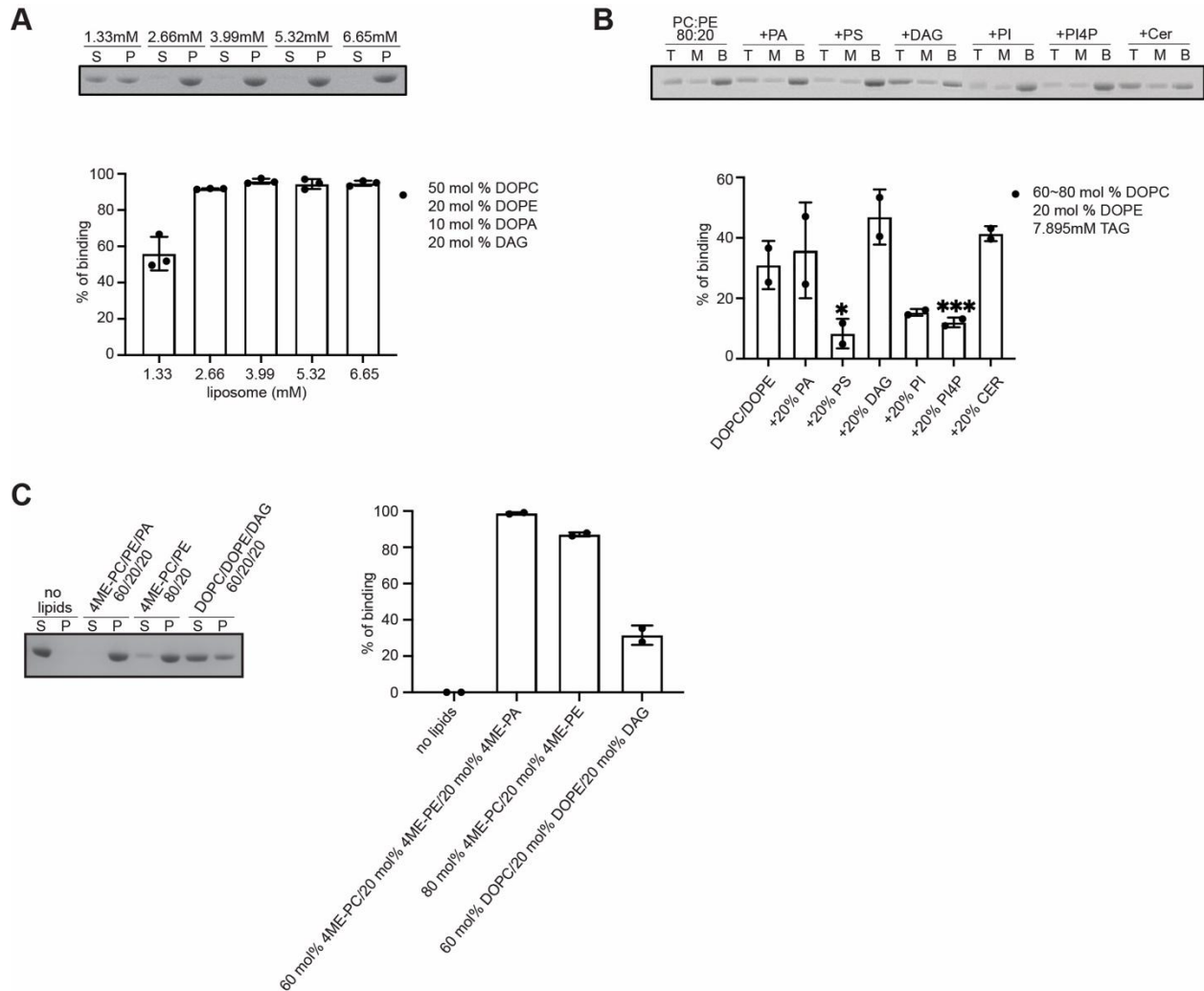


1289
 1290
 1291
 1292
 1293
 1294
 1295
 1296
 1297
 1298
 1299

Supplementary Figure 1.

A) DLS analysis of liposomes with different lipid composition. For each liposome, three measurements were plotted.

B-F) DLS analysis of different liposomes with or without full length PLIN3. For each liposome, the number average size distribution (%) was recorded and plotted (n=3) in the presence and absence of full length PLIN3.



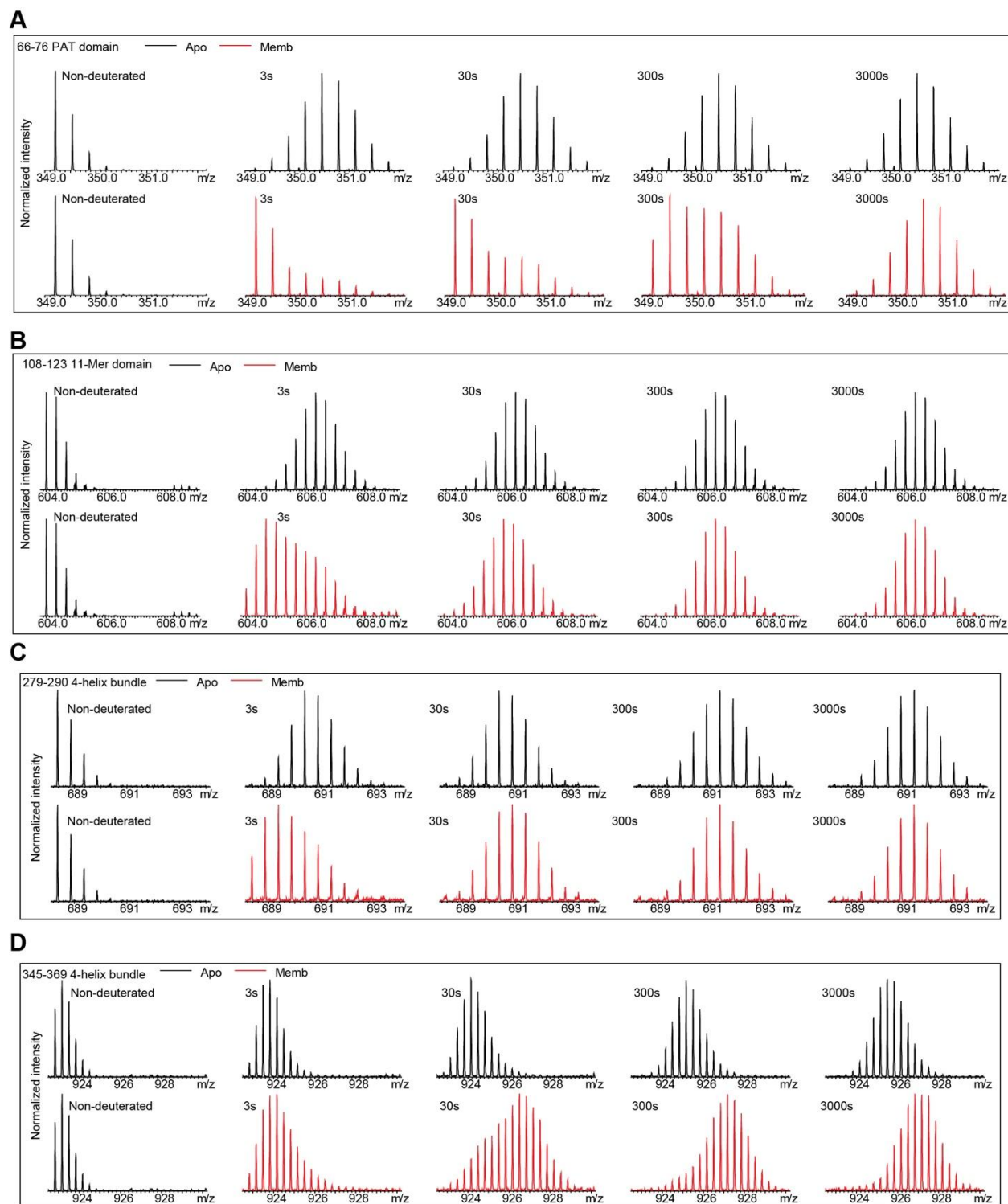
1300
1301
1302
1303
1304
1305
1306
1307
1308
1309
1310
1311
1312
1313
1314
1315
1316
1317
1318
1319

Supplementary Figure 2.

A) SDS-PAGE and quantitative analysis of human PLIN3 recruitment by increasing the total amount of liposomes. The molar ratio of DOPC/DOPE/DOPA/DAG in 50:20:10:20 was kept same. Lane S represents unbound human PLIN3 from supernatant. Lane P represents pelleted human PLIN3 that bound to liposomes. Bar graph shows total increase in liposome amount results almost 100% recruitment of PLIN3 to liposome.

B) SDS-PAGE and quantitative analysis of human PLIN3 recruitment to ALDs generated with DO-phospholipids and TAGs (C16) by adding additional with 20 mol% of lipids such as PS, PA, DAG, PI, PI4P and ceramide. Top, middle and bottom fractions after sucrose-gradient centrifuge were indicated as T, M and B, respectively. Statistical analysis was performed using ordinary one-way ANOVA with Tukey's multiple comparison test (n=2, *, p=0.0258, ***, p=0.004).

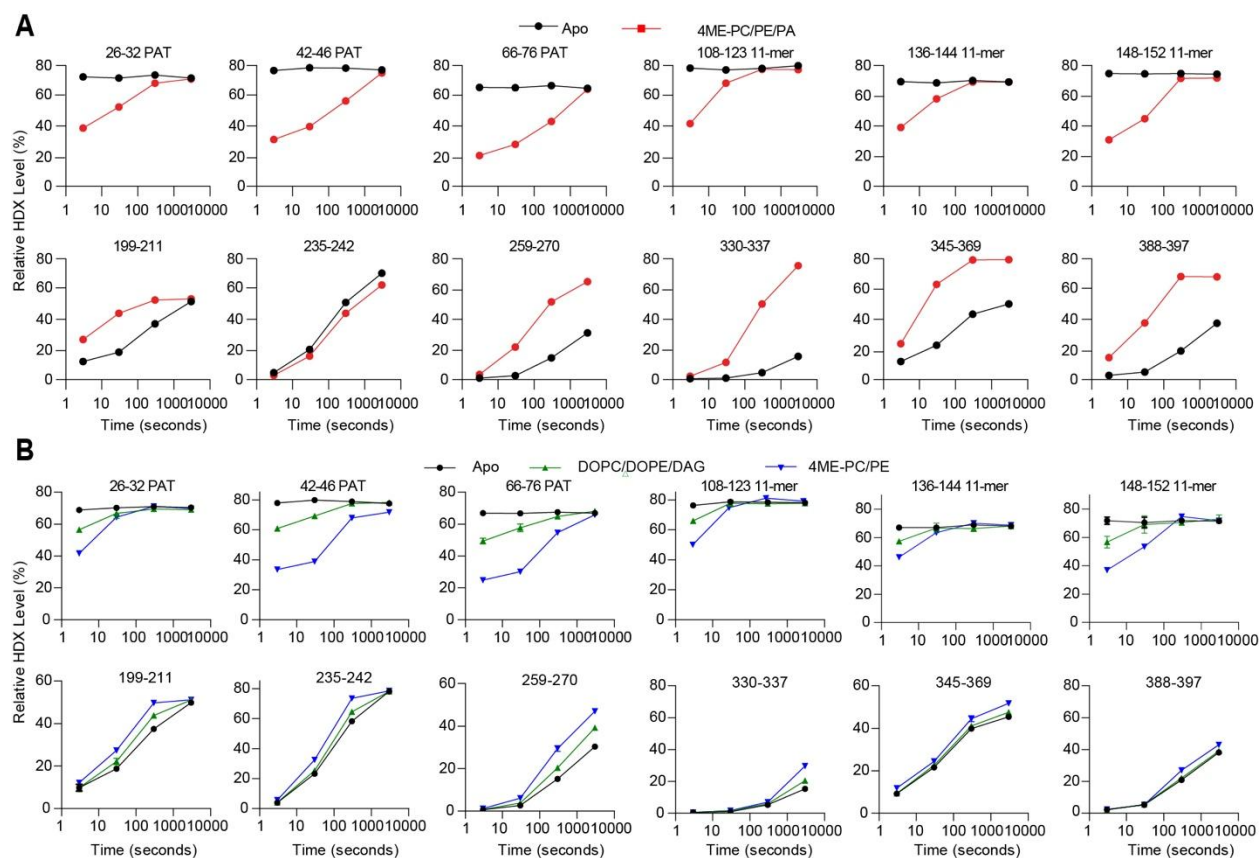
C) SDS-PAGE and quantitative analysis of human PLIN3 recruitment to liposomes in buffer containing 100mM NaCl and 20mM HEPES pH 7.0. Three different liposomes that were applied in HDX-MS were generated. Lane S represents unbound human PLIN3 from supernatant. Lane P represents pelleted human PLIN3 that bound to liposomes.



1320
1321
1322
1323
1324

Supplementary Figure 3.

Representative bimodal distribution mass spectra from the peptides at PAT domain, 11-mer repeats, and 4-helix bundle of PLIN3 after deuterium exchange.

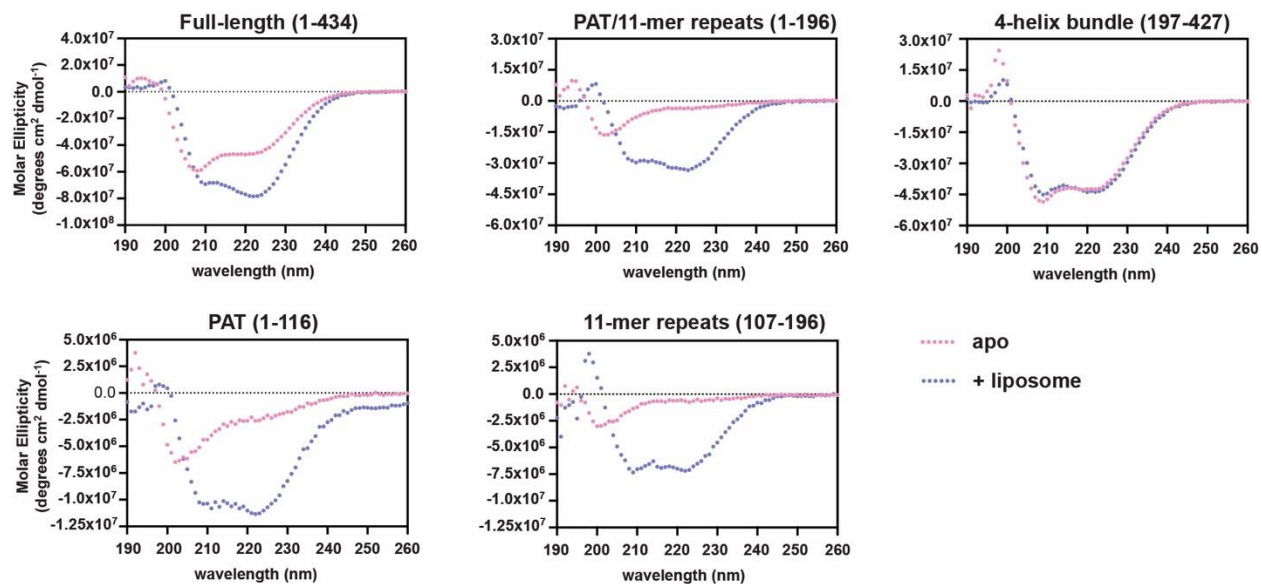


1325
1326
1327
1328
1329
1330
1331
1332
1333
1334
1335
1336
1337
1338
1339
1340
1341
1342
1343
1344
1345
1346
1347
1348
1349
1350

Supplementary Figure 4.

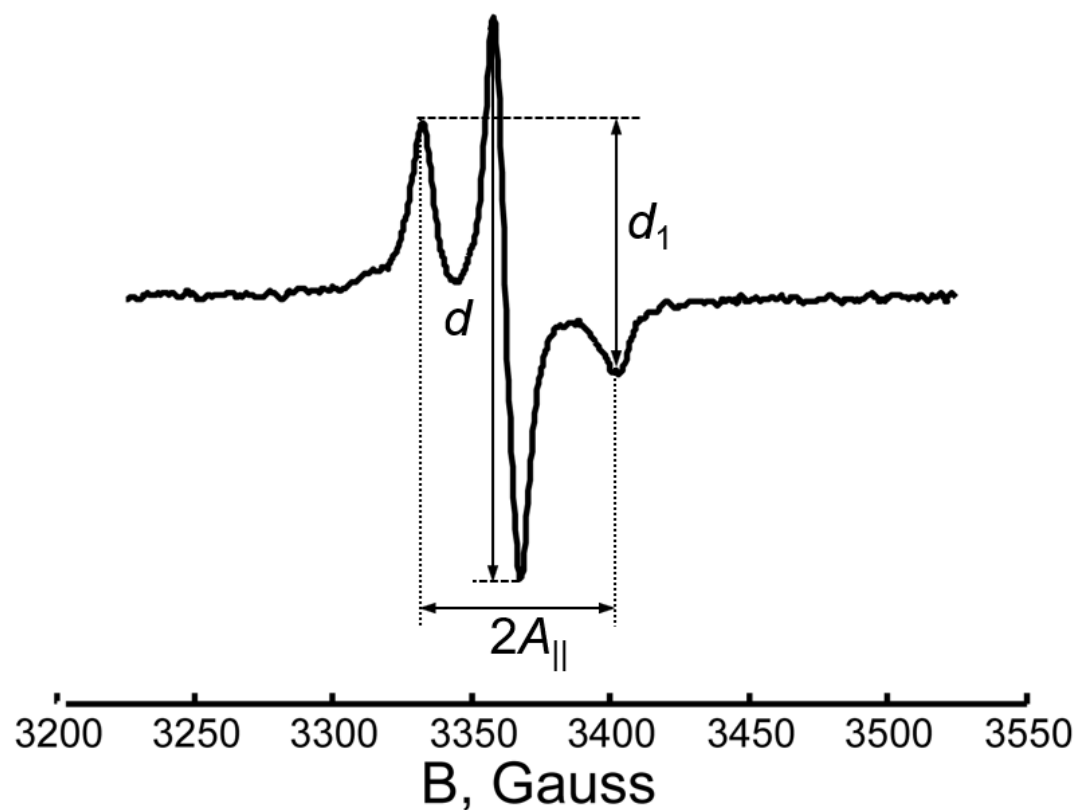
A) Deuterium exchange uptake plots for selected peptides in the PAT domain, 11-mer repeats and 4-helix bundle were plotted across all timepoints as 3s, 30s, 300s and 3000s. Data points in the absence and presence of liposomes were colored in black and red, respectively. Liposomes were generated with 60 mol% 4ME-PC, 20 mol% 4ME-PE and 20 mol% 4ME-PA). All peptides are shown in the source data.

B) Deuterium exchange uptake plots for selected peptides in the presence of two different liposomes are plotted across all timepoints as 3s, 30s, 300s and 3000s colored according the the legend. All peptides are shown in the source data.

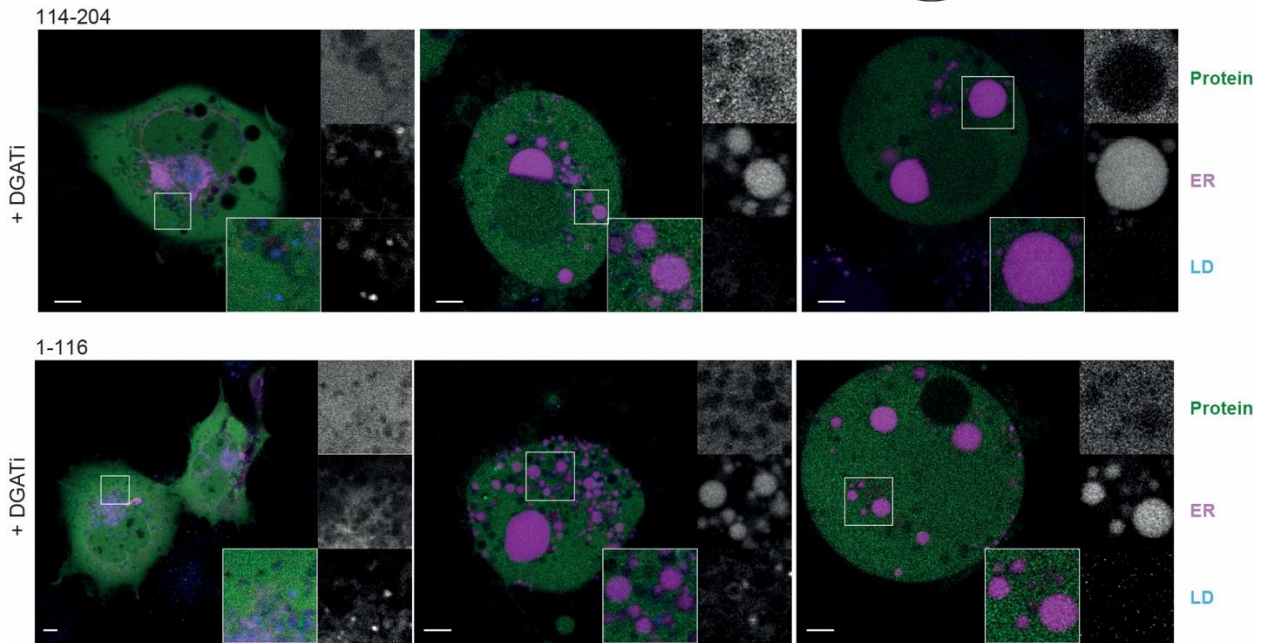
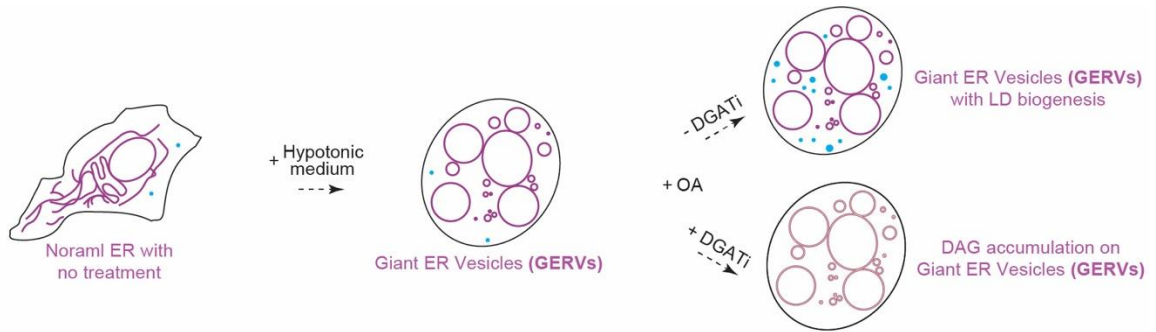


1351
1352
1353
1354
1355
1356
1357
1358
1359
1360

Supplementary Figure 5. CD analysis of PLIN3 full length and various fragments with or without 4ME-PC/PE/PA liposomes



1361 **Supplementary Figure 6.** CW ESR spectrum of 37C/144C in lipid recorded at 9,434 GHz
1362 frequency. The Parameter Δ , defined [99] as the ratio of d_1/d , is 0.45, which for the MTSL spin
1363 label indicates the distance in range of 1.5-2.0 nm [99, 100], i.e. somewhat shorter than
1364 reported by DEER which has reduced sensitivity to distances below 2.0 nm.
1365
1366
1367
1368
1369
1370
1371
1372
1373
1374
1375
1376
1377
1378
1379
1380
1381
1382
1383



1384
1385
1386
1387
1388
1389
1390
1391
1392
1393
1394
1395
1396
1397
1398
1399
1400
1401
1402
1403
1404
1405
1406

Supplementary Figure 7.

Subcellular localization of GFP tagged 114-204 and 1-116 constructs of PLIN3 was visualized in Cos7 cells under fluorescent microscope ZEISS LSM800 Airyscan. ER was visualized with ER specific marker RFP-KDEL in magenta. Lipid droplets were labeled with LipidTox Deepred to stain neutral lipids in cyan. After treated with hypotonic medium, cells were supplemented with oleate in the presence or absence of DGAT1/2 inhibitors.

1407
1408

Supplementary Table 1.
Summary of all HDX-MS data processing.

Data set	PLIN3 order disorder Expt-1	PLIN3 Apo Expt-2	PLIN3 + 60% 4ME-PC, 20% 4ME-PE, 20% 4ME-PA liposomes Expt-2	PLIN3 Apo Expt-3	PLIN3 + 60% DOPC, 20% DOPE, 20% DAG liposomes Expt-3	PLIN3+ + 80% 4ME-PC, 20% 4ME-PE liposomes Expt-3
HDX reaction details	%D ₂ O=84.9 % pH(read)=7.5 Temp=20°C	%D ₂ O=63% pH(read)=8.0 Temp=20°C	%D ₂ O=63% pH(read)=8.0 Temp=20°C	%D ₂ O=72% pH(read)=8.0 Temp=20°C	%D ₂ O=72% pH(read)=8.0 Temp=20°C	%D ₂ O=72% pH(read)=8.0 Temp=20°C
HDX time course (seconds)	0.3s, fully deuterated	3s, 30s, 300s, 3000s	3s, 30s, 300s, 3000s	3s, 30s, 300s, 3000s	3s, 30s, 300s, 3000s	3s, 30s, 300s, 3000s
HDX controls	FD	N/A	N/A	N/A	N/A	N/A
Back-exchange	Corrected by fully deuterated sample	No correction, deuterium levels are relative	No correction, deuterium levels are relative	No correction, deuterium levels are relative	No correction, deuterium levels are relative	No correction, deuterium levels are relative
Number of peptides	144	90	90	90	90	90
Sequence coverage	99.8%	91.7%	91.7%	91.7%	91.7%	91.7%
Average peptide /redundancy	Length= 17.3 Redundancy = 5.4	Length= 13.0 Redundancy = 2.6	Length= 13.0 Redundancy = 2.6	Length= 13.0 Redundancy = 2.6	Length= 13.0 Redundancy = 2.6	Length= 13.0 Redundancy = 2.6
Replicates	3	3	3	3	3	3
Repeatability	Average StDev=0.4%	Average StDev=0.6%	Average StDev=0.6%	Average StDev=0.8%	Average StDev=1.0%	Average StDev=0.9%
Significant differences in HDX	N/A	>5% and >0.4 Da and unpaired t-test ≤0.01	>5% and >0.4 Da and unpaired t-test ≤0.01	>5% and >0.4 Da and unpaired t-test ≤0.01	>5% and >0.4 Da and unpaired t-test ≤0.01	>5% and >0.4 Da and unpaired t-test ≤0.01
Data set	PLIN3 order disorder Expt-1	PLIN3 Apo Expt-2	PLIN3 + 60% 4ME-PC, 20% 4ME-PE, 20% 4ME-PA liposomes Expt-2	PLIN3 Apo Expt-3	PLIN3 + 60% DOPC, 20% DOPE, 20% DAG liposomes Expt-3	PLIN3+ + 80% 4ME-PC, 20% 4ME-PE liposomes Expt-3
HDX	%D ₂ O=84.9	%D ₂ O=63%	%D ₂ O=63%	%D ₂ O=72%	%D ₂ O=72%	%D ₂ O=72%

reaction details	% pH _(read) =7.5 Temp=20°C	pH(read)=8.0 Temp=20°C	pH(read)=8.0 Temp=20°C	pH _(read) =8.0 Temp=20°C	pH _(read) =8.0 Temp=20°C	pH _(read) =8.0 Temp=20°C
HDX time course (seconds)	0.3s, fully deuterated	3s, 30s, 300s, 3000s	3s, 30s, 300s, 3000s	3s, 30s, 300s, 3000s	3s, 30s, 300s, 3000s	3s, 30s, 300s, 3000s
HDX controls	FD	N/A	N/A	N/A	N/A	N/A
Back-exchange	Corrected by fully deuterated sample	No correction, deuterium levels are relative	No correction, deuterium levels are relative	No correction, deuterium levels are relative	No correction, deuterium levels are relative	No correction, deuterium levels are relative
Number of peptides	144	90	90	90	90	90
Sequence coverage	99.8%	91.7%	91.7%	91.7%	91.7%	91.7%
Average peptide /redundancy	Length= 17.3 Redundancy = 5.4	Length= 13.0 Redundancy = 2.6	Length= 13.0 Redundancy = 2.6	Length= 13.0 Redundancy = 2.6	Length= 13.0 Redundancy = 2.6	Length= 13.0 Redundancy = 2.6
Replicates	3	3	3	3	3	3
Repeatability	Average StDev=0.4%	Average StDev=0.6%	Average StDev=0.6%	Average StDev=0.8%	Average StDev=1.0%	Average StDev=0.9%
Significant differences in HDX	N/A	>5% and >0.4 Da and unpaired t-test ≤0.01	>5% and >0.4 Da and unpaired t-test ≤0.01	>5% and >0.4 Da and unpaired t-test ≤0.01	>5% and >0.4 Da and unpaired t-test ≤0.01	>5% and >0.4 Da and unpaired t-test ≤0.01
Data set	PLIN3 order disorder Expt-1	PLIN3 Apo Expt-2	PLIN3 + 60% 4ME-PC, 20% 4ME-PE, 20% 4ME-PA liposomes Expt-2	PLIN3 Apo Expt-3	PLIN3 + 60% DOPC, 20% DOPE, 20% DAG liposomes Expt-3	PLIN3+ + 80% 4ME-PC, 20% 4ME-PE liposomes Expt-3
HDX reaction details	%D2O=84.9 % pH(read)=7.5 Temp=20°C	%D2O=63% pH(read)=8.0 Temp=20°C	%D2O=63% pH(read)=8.0 Temp=20°C	%D2O=72% pH(read)=8.0 Temp=20°C	%D2O=72% pH(read)=8.0 Temp=20°C	%D2O=72% pH(read)=8.0 Temp=20°C
HDX time course (seconds)	0.3s, fully deuterated	3s, 30s, 300s, 3000s	3s, 30s, 300s, 3000s	3s, 30s, 300s, 3000s	3s, 30s, 300s, 3000s	3s, 30s, 300s, 3000s
HDX controls	FD	N/A	N/A	N/A	N/A	N/A
Back-exchange	Corrected by fully	No correction,	No correction,	No correction,	No correction,	No correction,

	deuterated sample	deuterium levels are relative	deuterium levels are relative	deuterium levels are relative	deuterium levels are relative	deuterium levels are relative
Number of peptides	144	90	90	90	90	90
Sequence coverage	99.8%	91.7%	91.7%	91.7%	91.7%	91.7%
Average peptide /redundancy	Length= 17.3 Redundancy = 5.4	Length= 13.0 Redundancy = 2.6	Length= 13.0 Redundancy = 2.6	Length= 13.0 Redundancy = 2.6	Length= 13.0 Redundancy = 2.6	Length= 13.0 Redundancy = 2.6
Replicates	3	3	3	3	3	3
Repeatability	Average StDev=0.4%	Average StDev=0.6%	Average StDev=0.6%	Average StDev=0.8%	Average StDev=1.0%	Average StDev=0.9%
Significant differences in HDX	N/A	>5% and >0.4 Da and unpaired t-test ≤ 0.01	>5% and >0.4 Da and unpaired t-test ≤ 0.01	>5% and >0.4 Da and unpaired t-test ≤ 0.01	>5% and >0.4 Da and unpaired t-test ≤ 0.01	>5% and >0.4 Da and unpaired t-test ≤ 0.01

1409